minerals

MDPI

Article

Actualistic Testing of the Influence of Groundwater Chemistry on Degradation of Collagen I in Bone

Paul V. Ullmann [1,*], Kristyn K. Voegele [1] and Kenneth J. Lacovara [1,2]

[1] Department of Geology, Rowan University, Glassboro, NJ 08028, USA
[2] Jean and Ric Edelman Fossil Park, Rowan University, Sewell, NJ 08080, USA
* Correspondence: ullmann@rowan.edu

Abstract: Recent experiments have heightened our understanding of reactions which can stabilize biomolecules during early diagenesis, yet little remains known about how groundwater chemistry can aid or hinder molecular preservation within a bone through geologic time. To elucidate this issue, we conducted actualistic experiments of bone decay employing varied fluid compositions to simulate a suite of groundwaters. Modern domestic chicken (*Gallus gallus*) femora were placed in a matrix of compositionally- and texturally-mature, fluvially-deposited sand. To simulate groundwater flow, deionized water or solutions enriched in calcium carbonate, phosphate, or iron were percolated through separate trials for a period of 90 days. After completion of the experiment, degradation of the bones was examined via histologic thin sectioning and two immunoassays against collagen I, the primary bone structural protein: immunofluorescence and enzyme-linked immunosorbent assay. Collagen loss was found to be greatest in the iron trial and least in the calcium carbonate trial, the latter of which experienced partial permineralization with calcite over the course of the experiment. Specifically, the iron trial was found to retain only ~35 ng of collagen I per 100 ng of protein extract, whereas the calcium carbonate trial retained ~90 ng of collagen I. Further, in the iron and calcium carbonate trials, cementation of sediment onto bone surfaces preferentially occurred over more porous regions of the epiphyses, perhaps stimulated by greater release of decay compounds from these regions of the bones. Of the two trials exhibiting intermediate results, the phosphate trial induced slightly greater decay of collagen than the deionized water control, which retained ~60 ng and ~80 ng of collagen I per 100 ng of protein extract, respectively. These results demonstrate that highly acidic conditions during early diagenesis can overwhelm any preservative effects of free radical-mediated stabilization reactions, whereas early-diagenetic permineralization can drastically slow biomolecular decay (ostensibly by hampering microbial access to the interior of a bone), thereby increasing the likelihood of a bone to retain biomolecules and/or their decay products through protracted diagenesis. Future variations of this actualistic experiment employing varied durations, solute concentrations, bacterial communities, pH values, and/or host sediments could provide further important insights into the ways in which early-diagenetic environments control the initial decay of biomolecules within bone and other tissues.

Keywords: actualistic taphonomy; bone; calcium carbonate; collagen; diagenesis; fossilization; iron; molecular paleontology; phosphate

Citation: Ullmann, P.V.; Voegele, K.K.; Lacovara, K.J. Actualistic Testing of the Influence of Groundwater Chemistry on Degradation of Collagen I in Bone. *Minerals* **2023**, *13*, 596. https://doi.org/10.3390/min13050596

Academic Editors: Pedro Álvarez-Lloret and Yannicke Dauphin

Received: 27 February 2023
Revised: 5 April 2023
Accepted: 21 April 2023
Published: 25 April 2023

1. Introduction

Discovery of endogenous biomolecules in fossil bones, including DNA and proteins such as collagen I and osteocalcin, has become increasingly common over the last two decades (e.g., [1–16]) (Figure 1). These discoveries challenge long-held presumptions about the nature of fossilization and provide intriguing means of advancing several lines of current research, including: (1) identifying indeterminate fossil remains (e.g., [17,18]); (2) testing of phylogenetic hypotheses independent of skeletal morphology (e.g., [4,11,19–24]); (3) calibration of molecular clocks for cladistic analyses (e.g., [20,23–25]); (4) tracking the

genetic and phylogeographic history of past populations (e.g., [26–28]); and (5) examining trajectories of molecular evolution and the physiology of extinct taxa (e.g., [29]).

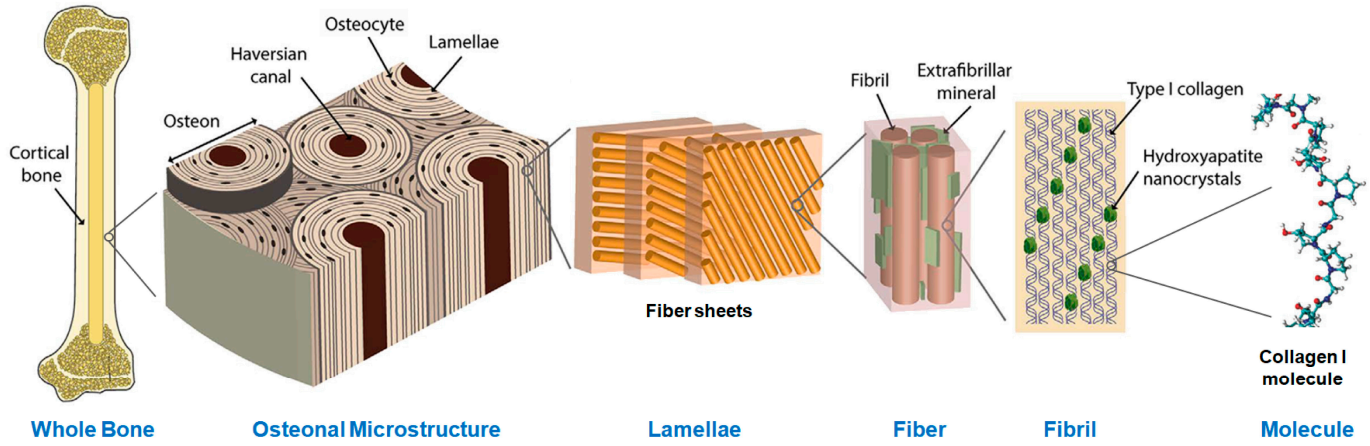

Figure 1. The hierarchical structure of bone from the histological to the molecular level. The structural protein collagen I, shown at far right, forms the majority of the soft-tissue matrix of bone tissue. Modified from Zimmerman et al. [30] under a CC BY-4.0 license.

Before we can exploit the full molecular potential of the fossil record, it is first imperative to clarify preservation mechanisms which can account for biomolecular preservation within fossils over geologic timescales. Further, to reach that goal, we must first achieve a better understanding of the factors involved in cellular/soft tissue decay and stabilization during diagenesis and their relative importance in varied depositional environments. For example, groundwater composition, flow rate, and pH, as well as temporal fluctuations in these variables, are all known to mediate diagenetic alteration of bone as an ultrastructural tissue after it is buried in sedimentary environments [31–36], but the influences of these variables on biomolecular decay and stabilization have largely yet to be empirically tested.

One fruitful means of exploring how taphonomic variables influence molecular decay is to model decay and fossilization processes in the laboratory through actualistic experimentation [37]. Experimental recreation of decay and fossilization pathways allows one to control and reduce the number of independent variables and evaluate physicochemical processes in a manner not achievable by direct study of ancient fossils. For example, actualistic studies have advanced understanding of how microbes may mediate permineralization of bone [38,39], how fluvial currents winnow mass death assemblages of skeletons (e.g., [40]) or impart directionality patterns to fossil assemblages (e.g., [41,42]), and how bone adsorbs trace elements from environmental waters after death and skeletonization [43,44].

We present results of a novel actualistic experiment conducted to explore the influence of groundwater chemistry on protein decay. Building on the methods developed by Carpenter [38], Daniel and Chin [39], and Peterson et al. [45], bones were placed within a sedimentary matrix and exposed to a simulated groundwater for a period of 90 days. Our simulated groundwater solutions included calcium carbonate supersaturation, enrichment in dissolved phosphate, and enrichment in ferric iron, along with a deionized water control. These choices were made with the intent of modeling initial decay after burial in conditions similar to (but intensified from) those within a diverse suite of natural environments, so that the results may inform molecular paleontologists working with vertebrate fossils preserved under diverse depositional circumstances. This study includes the first utilization of immunoassays in an actualistic simulation of bone diagenesis, thus providing molecular taphonomists with a novel foundation for further actualistic testing of biomolecular decay and stabilization pathways.

2. Materials and Methods

2.1. Materials

All expendable materials used in construction of the trial apparatuses were purchased new. These included silicone tubing, silicone, cellophane, faucet aerators, steel wool, aluminum foil, lab spatulas, polyethylene screw-top caps from 50 mL centrifuge tubes, and 60 mL polypropylene syringes. All reagents used to make solutions were acquired from Sigma, namely calcium carbonate (Sigma-12010), phosphoric acid (Sigma-466123), and iron III chloride (Sigma-157740). Borosilicate glass media-storage bottles (1 L) were sequentially washed with 100% bleach then 95% ethanol, then autoclaved prior to use. Chicken (*Gallus gallus*) thighs were purchased from a local grocery store, from which the femora were extracted with disposable sterile scalpels. Because rapid burial is rare and the most common taphonomic circumstance is for bones to be buried after skeletonization and at-least brief subaerial exposure/decay [46–49], the femora were degreased in a 10% Shout^{TM} solution by rocking in separate 600 mL Erlenmeyer flasks for 48 h (with three changes, following the method of [50]). After degreasing, bones were thoroughly rinsed in deionized water and stored at 4 °C overnight before use in the trials.

Natural, fluvially-deposited sand was collected from a south-facing cutbank exposure along the Mullica River in southern New Jersey (39°44′02.83″ N, 74°42′40.33″ W) to serve as a realistic and permeable sedimentary matrix. The Mullica River was chosen due to accessibility, the high compositional and textural maturity of the unconsolidated sediments forming its banks, and the limited extent of human development along much of its length (in an effort to acquire a sediment sample that was as free from anthropogenic physical and chemical influences as possible). Regionally, the Mullica River is considered one of the most pristine, undisturbed fluvial systems in the northeastern United States [51], where it is commonly used as an 'uncontaminated' reference for regional water-quality studies (e.g., [52,53]). Sand was collected from just above, at, and beneath the current sediment-water interface and passed through a 1 mm sieve to remove any organic particulates and homogenize the sand sample for use in our trials. Because bones buried in natural environments are exposed to bacteria and other microbes in soils/sediments, no effort was made to sterilize the sand (i.e., we did not treat the sand with sodium azide or bleach).

2.2. Methods

2.2.1. Trial Apparatus

Our trial apparatus design (Figure 2) was inspired by that of Daniel and Chin [39] (which was in-turn inspired by [38]). Nitrile gloves were worn during the construction of each identical apparatus to limit the input of exogenous microbes and/or other contaminants. 60 mL polypropylene syringes (with plungers removed) were utilized as a sterile incubation chamber for each trial. To ensure sand would not pass through the base of the syringes, a small tuft of autoclave-sterilized steel wool was placed in the bottom of each syringe, then covered by an autoclaved faucet aerator (i.e., a fine stainless-steel mesh). Roughly 10 mL of sand was then added to each syringe, a femur was placed in each with the distal end directed down, and ~35 mL of additional sand was packed around and over the top of each femur with a disposable, sterile lab spatula. A small tuft of steel wool was then placed over the sand to disperse solution drips so that their impacts would not 'excavate' a depression in the sand down to the proximal end of the bone. A lid for each trial chamber was prepared by drilling a 7 mm-diameter hole (with an autoclave-sterilized drill bit) in the center of a polyethylene screw-top cap from a 50 mL centrifuge, then attaching it to the syringe with clear 100% silicone. The assembled trial chambers were suspended upright from ring stands via ring clamps. 600 mL beakers were placed under each syringe to collect effluent solution, which was emptied every ~48 h. Prepared "groundwater" solutions (in 1 L jars) were placed beside the trial apparatuses and fed via 6.4 mm-diameter silicone tubing through a peristaltic pump and into assigned trial chambers (Figures 2 and 3). Each silicone tube was then sealed into the respective lid of its trial chamber using 100% silicone. To limit influx of airborne contaminants, cellophane was tightly wrapped over the top of

each solution feeder jar and each gap between syringe and effluent beaker (under each trial apparatus). Finally, aluminum foil was wrapped around each incubation chamber and each solution feeder jar to simulate the darkness of burial.

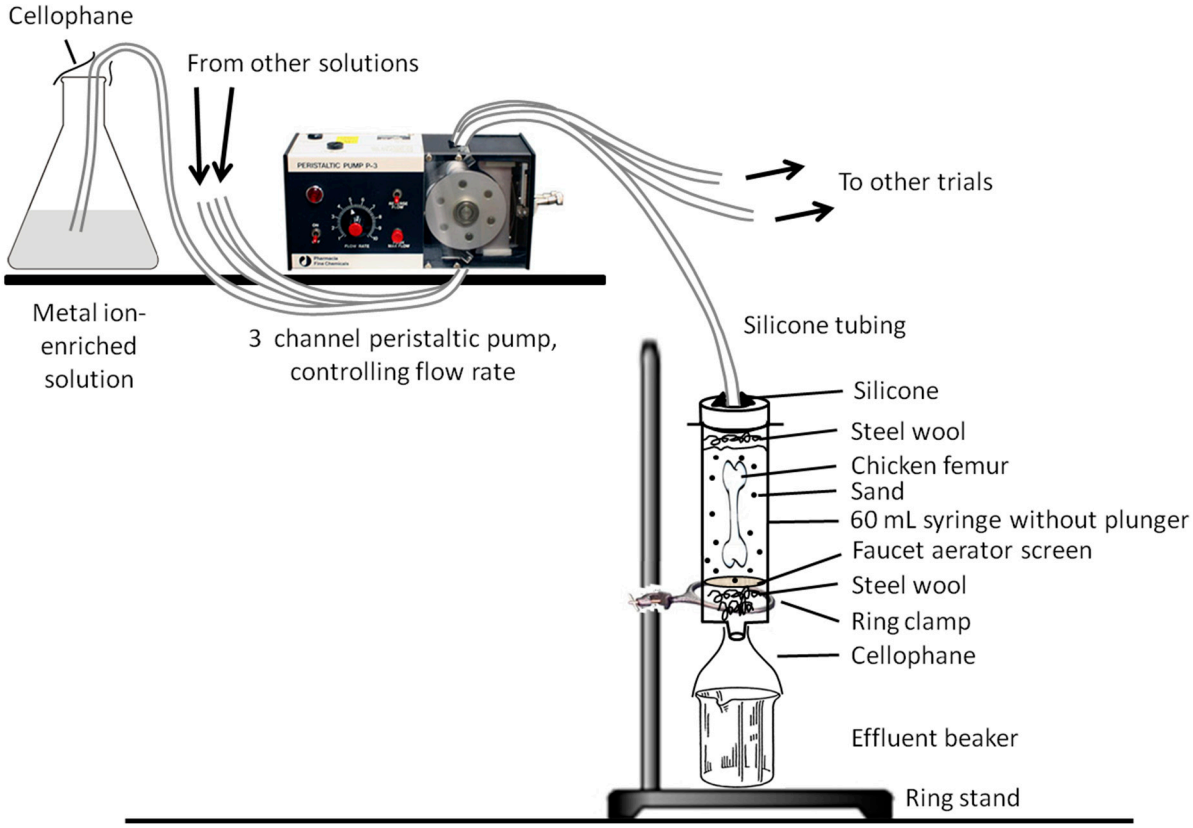

Figure 2. Schematic representation of the experimental apparatus. The general template of this design was inspired by that used by Daniel and Chin [39].

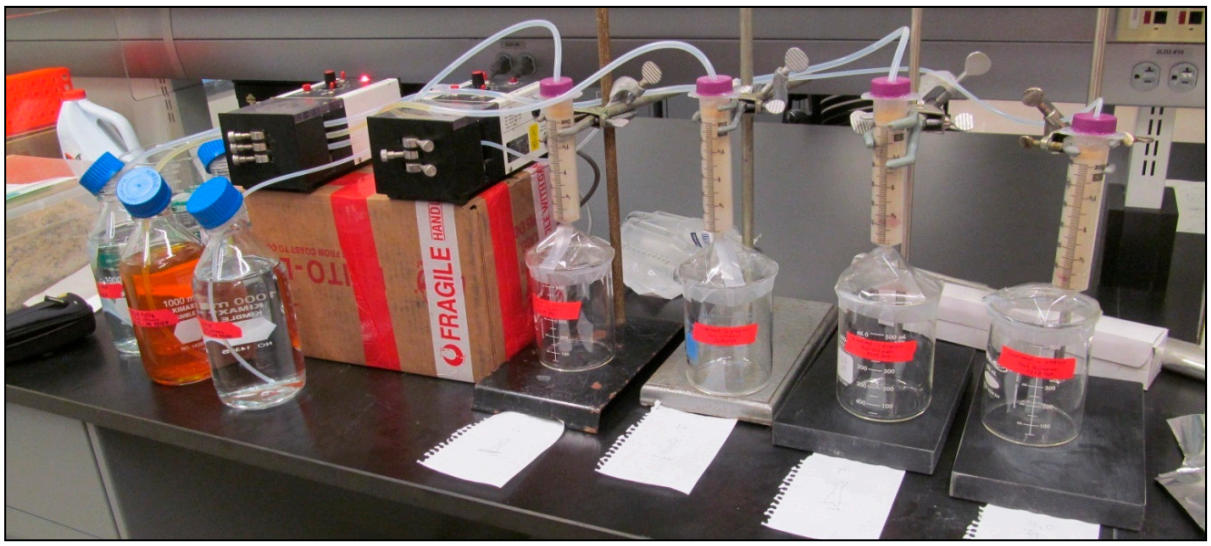

Figure 3. Initial setup of the experiment, prior to wrapping each of the bone/sediment trial chambers and solution bottles with aluminum foil (to simulate darkness of burial). Peristaltic pumps (middle, on top of box) fed simulated groundwater solutions from storage bottles at left to separate incubation chambers at right. Effluent solutions were collected in the beakers beneath each incubation chamber.

2.2.2. Solutions and Trials

While our methods could be utilized to explore the influences of a wide variety of potential variables, we elected to focus on the influence of groundwater enrichment in metals commonly involved in fossilization. Pore fluid enrichment with metals is an intriguing variable to examine because the presence of metal cations has been found to inhibit autolytic enzymes [54,55], which could hypothetically elevate biomolecular preservation potential within a bone as it is fossilizing. Therefore, to test the influence of groundwater enrichment in various metals on protein decay, we made three simulated "groundwater" solutions enriched in either calcium carbonate ($CaCO_3$), phosphate (PO_4), or ferric iron (Fe^{+3}), and compared results from those trials to a deionized water control. Aqueous solutions of the first three of these solutions were made by solubilization of reagent salts.

Calcium carbonate was chosen for examination because: (1) calcium is a primary component of bone hydroxyapatite [56] and an essential metal nutrient sought by microbial decomposers [57,58]; (2) calcite is a common cementing mineral and permineralizing phase in clastic sedimentary environments (e.g., [59–61]); and (3) microbially-mediated permineralization of bone with calcium carbonate could ostensibly lead to rapid equilibration with the early-diagenetic environment [39], thereby promoting biomolecular stabilization in a bone after burial. In an attempt to initiate incipient permineralization over the timeframe of an actualistic experiment, we followed the protocol of Daniel and Chin [39] to prepare a supersaturated solution of $CaCO_3$. This solution was prepared by dissolving 2 g of $CaCO_3$ into 1 L of 0 °C deionized water (i.e., $CaCO_3$ powder dissolved into solution as the water melted), which was then titrated to pH 6.5 with 1 N hydrochloric acid (HCl). Freezing of the water and titration to acidic pH were necessary to enhance calcium carbonate solubilization because $CaCO_3$ solubility increases with decreasing temperature and pH [62]. The prepared solution was filtered (using a disposable 0.22 µm screw-top filter) to remove any remaining undissolved $CaCO_3$, bringing it to a final concentration of ~0.67 g/L. This is nearly twice natural saturation (0.3 g/L at pH 6.5 [39]).

Iron was also chosen for investigation because: (1) iron is common in terrestrial surface and groundwaters (e.g., [63,64]); (2) iron carbonates (e.g., siderite) and oxides (e.g., goethite) are common permineralizing phases in clastic sedimentary environments (e.g., [59,65–67]); and (3) it has been hypothesized that iron released from decaying hemoglobin and myoglobin can catalyze free-radical reactions which may stabilize soft tissues and their component biomolecules by inducing inter- and intramolecular crosslinking during early diagenesis [68–70]. For this trial, a 10 mM iron chloride ($FeCl_3$) solution was prepared following the protocol of Ferris et al. [71]. This solution was prepared by dissolving 1.62 g of FeCl3 in 1 L of water in a laminar-flow hood at room temperature (RT), then filtering the solution (0.22 µm) to remove any undissolved iron chloride.

Finally, phosphate was chosen for investigation because phosphate: (1) is the second primary component of bone hydroxyapatite [56]; (2) is another essential metal nutrient sought by microbial decomposers [57,58,72,73]; and (3) precipitation of secondary authigenic phosphate is known to contribute to "replication" of ultrastructural soft tissues in vertebrate remains (e.g., [74–79]). Since we could find no previous attempts at modeling a groundwater enriched with phosphate in prior literature, we decided that a conservative starting point would be to prepare a solution to twice maximum-reported natural abundance. Sheldon [80] reported that the concentration of phosphorus in natural sedimentary pore fluids can be as high as 9 mg/L (0.29 mM), so we prepared a solution to 18 mg/L (58 mM) using phosphoric acid (H_3PO_4). This solution was prepared by dissolving 56 mg of crystalline H_3PO_4 per 1 L of deionized water. Since this would make an unnaturally acidic solution, the pH was raised back to 7.0 through addition of a few drops of 6 N sodium hydroxide (NaOH) solution. The final pH-balanced solution did not require filtration as the phosphate concentration remained far below saturation.

Fresh solutions were prepared every 3–4 days and continually fed to each trial by two three-channel peristaltic pumps (Pharmacia model P-3) which were calibrated to matching

flow rates of 1 L/day (=0.7 mL/min) (Figure 3). This rate equates to ~1.63 m/day, which falls well within the range of flow rates of natural aquifers (0.025–15 m/day; [39] and references therein).

After completion of the experiment, the contents of each trial chamber were removed and the bones photographed. We then described their general state of decay and, with separate, sterile, disposable scalpels, divided the shaft of each femur into three sections for (1) resin embedding and histologic sectioning; (2) protein extraction; and (3) demineralization and immunofluorescence (Figure 4). This splicing revealed that white/gray-colored degradation products of medullary tissue remained within the shaft of each femur. These tissues, which were amorphous and generally consistent with the gelatinous nature of intensely decayed bone marrow (cf. [81]), were manually removed with sterile dissection probes prior to further examinations. Pliable, partially-decomposed periosteal linings were also immediately removed from each diaphyseal segment using separate, sterile disposable scalpels. Finalized diaphyseal samples designated for histology and protein extraction were then stored at −20 °C until further use, whereas those designated for immunofluorescence were demineralized in freshly-prepared 0.5 M ethylenediaminetetraacetic acid (EDTA) pH 8.0 (0.22 μm filtered) in new, autoclave-sterilized 20 mL glass scintillation vials for 2 weeks (with EDTA exchanged daily).

2.2.3. Histology

Traditional methods for bone embedding and sectioning were followed [82]. This first involved impregnation of designated diaphysis segments with Silmar 41^{TM} resin (US Composites, West Palm Beach, FL, USA) in a vacuum chamber for 7 min at 24 in Hg. After polymerization overnight at 4 °C then at RT for another 24 h, a precision wafer saw (Buehler IsoMet 1000) was used to cut 1.5 mm thick transverse sections of each respective diaphysis sample. Because bone tissues displayed a slightly pliable character at this stage, both faces of each thick section were lightly treated with PaleoBond Penetrant Stabilizer (Pb002) and allowed to dry overnight. One face of each section was then ground and polished with successively finer sandpapers (320 and 600 grits) on a Buehler EcoMet 4000 Grinder/Polisher. Polished slides were then adhered to frosted glass slides with two-ton Clear Weld^{TM} epoxy and allowed to dry overnight at RT. Mounted sections were then ground and polished as above to a final thickness of ~100 μm. Slides were optically examined and imaged via transmitted and polarized light using a Zeiss Axioskop 40 petrographic microscope with an attached AxioCam MRC5 camera.

2.2.4. Protein Extraction

All protein extractions and immunoassays characterizing the extent of decay of collagen I were performed in triplicate. We followed the sequential demineralization-based immunoprecipitation extraction protocol of Schroeter [83] for this study.

In brief, aliquots of 2 g of cortical bone were ground to fine powder (<1 mm grain size) in nitric-acid- and autoclave-sterilized mortar and pestles and added to separate 10 mL spin columns (Pierce) in 50 mL centrifuge tubes. Aliquots of sediment from each trial were also separately ground to serve as negative controls, and one additional spin column per column of bone powder was left empty to serve as a buffer ("blank") control. Columns were demineralized overnight at RT on a rocker with 10 mL of 0.6 M HCl, then centrifuged at 1000 rcf the following day to collect an 'HCl extract'. Demineralization was then continued with 10 mL of 4 M guanidine hydrochloride (GuHCl) in 0.05 M Tris pH 7.4, again incubating overnight on a rocker (this time at 65 °C). The next day, columns were centrifuged to collect a 'GuHCl extract'. Protein precipitation began with centrifugation (8000 rcf, 10 min) to pelletize any remaining undissolved solids. Resulting supernatants were then decanted into new 50 mL tubes for immunoprecipitation, which was performed for 1–1.5 h at 4 °C with 2.5 mL of 100% trichloracetic acid (TCA) for each HCl extract or overnight at −20 °C with 25 mL of 100% ethanol for each GuHCl extract. Precipitated HCl extracts were washed the following day by three rounds of centrifugation for 20 min (each

at 8500 rpm), decanting, and rinsing of the pellet with 5 mL of 100% acetone. Precipitated GuHCl extracts were washed by three rounds of centrifugation for 10 min, decanting, and rinsing of the pellet with 5 mL of 90% ethanol. After final centrifugation and decanting, tubes were inverted over paper towels in a laminar-flow hood to dry overnight at RT. Finalized extract tubes were then sealed and stored at −80 °C until analysis. 'GuHCl extract' fractions are expected to contain the majority of extracted collagen [15].

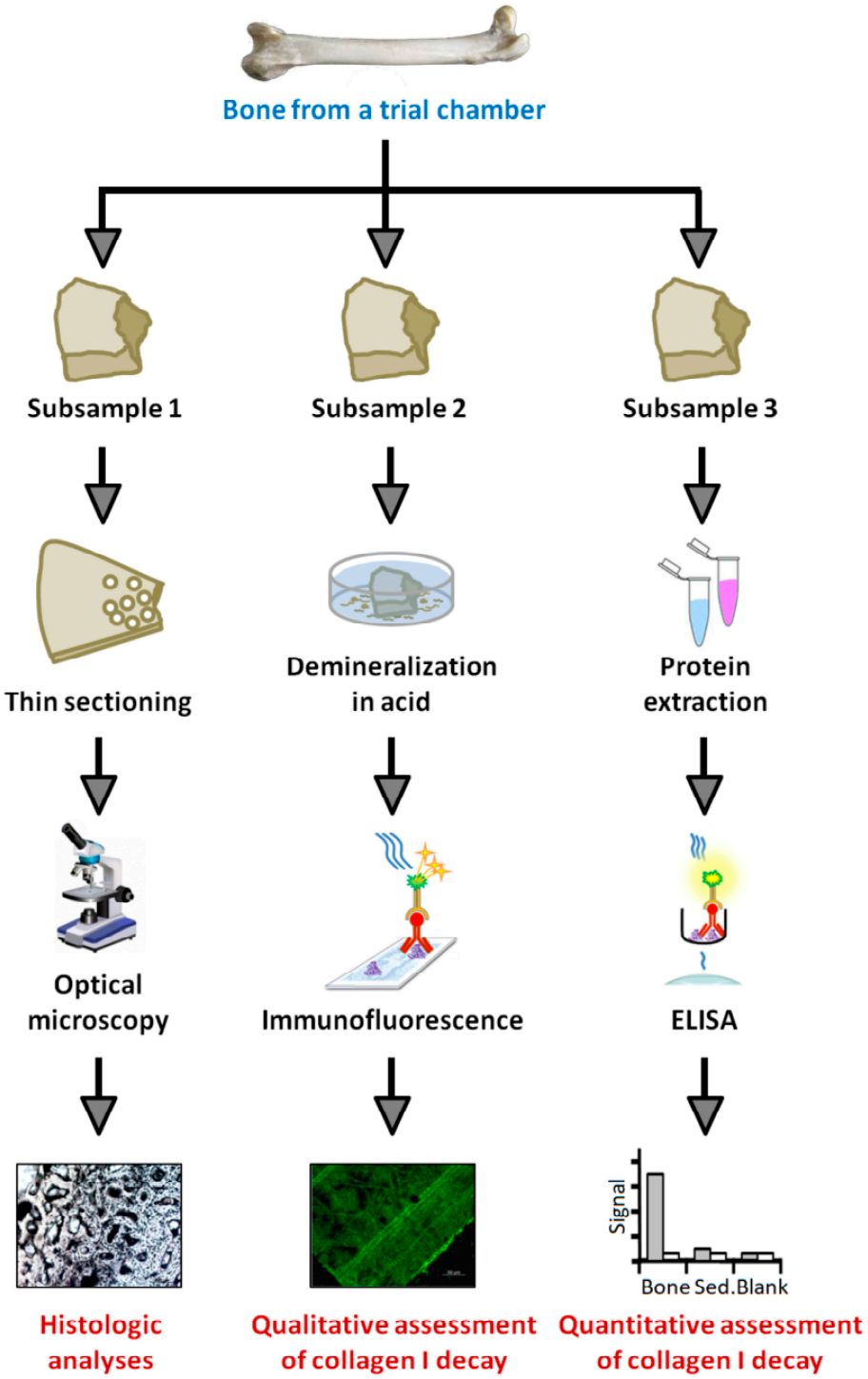

Figure 4. Flow chart depicting the analyses performed on each bone after completion of the experiment. Three portions of the shaft of each bone were excised for thin sectioning and histology (subsample 1), demineralization and in situ immunofluorescence (subsample 2), and protein extraction and enzyme-linked immunosorbent assay (ELISA; subsample 3).

2.2.5. ELISA

We followed the ELISA protocol of Zheng and Schweitzer [84]. In brief, precipitated extracts were resuspended in 1X phosphate buffered saline (PBS) to form 1 mg/mL stocks, which were then serially diluted to form 1 µg/mL stocks for plating. For the buffer control, 1 mL of PBS was added to each extraction blank tube and then immediately collected. Bone sample solutions and 1X PBS (for resuspension buffer control wells) were plated at 100 µL/well (=0.1 µg/well of sample) on a 96-well Immulon 2HB U-bottom microtiter plate (Thermo Scientific, Waltham, MA, USA). Solutions were discarded after this 4 h incubation at RT, as well as after each of the following steps (to remove any unbound antigens or antibodies). The plate was then incubated for 4 h at RT in 200 µL/well of ELISA blocking buffer (5% bovine serum albumin in 1X PBS with 2% Thimersol and 0.005% Tween 20) to avert non-specific binding. Polyclonal rabbit anti-chicken collagen I antibodies (U.S. Biological, Salem, MA, USA, C7510-13B), diluted to a concentration of 1:400 in blocking buffer, were then added to a subset of wells, whereas blocking buffer was added to control wells. After an overnight incubation at 4 °C, the plate was washed 10–15 times in ELISA wash buffer (10% PBS in Type I 18.2 Ω water with 0.1% Tween 20) and dried. Wells were then incubated for 2 h at RT in secondary antibodies (100 µL/well alkaline phosphatase-conjugated goat anti-rabbit IgG (H + L), Invitrogen G-21079) diluted 1:1000 in blocking buffer. The plate was then washed, dried, and 100 µL/well reading substrate (made by adding one tablet of 0.5 mM $MgCl_2$ + p-nitrophenylphosphate (Sigma N-9389) to 10 mL of 9.8% diethanolamine) was added. Absorbance values were read at 405 nm using a Molecular Devices THERMOmax microplate reader at the following time intervals: 0, 10, 20, 30, 40, 50, 60, 90, 120, 150, and 180 min. Secondary-only wells, which never received the primary antibody, were analyzed as additional controls to test for non-specific binding of secondary antibodies.

2.2.6. Immunofluorescence

Demineralized bone tissues were embedded, sectioned, and analyzed following the protocols of Zheng and Schweitzer [84] and Ullmann et al. [15]. This initially involved mincing of demineralized tissues with a sterile razor on a sterilized lab plate and rinsing of the minced products with Type 1 18.2 Ω water in sterile 1.5 mL centrifuge tubes. Minced tissues were then fixed for 1 h in 10% neutral buffer formalin pH 7.2 in 15 mL centrifuge tubes. After brief rinses in Type 1 18.2 Ω water, samples were transferred to new 15 mL centrifuge tubes and dehydrated in 70% ethanol. Resin impregnation then involved incubation for 1 h in a 2:1 solution of 70% ethanol/LR White™, after which the samples were transferred into 0.95 mL gelatin capsules filled with pure LR White™ (Electron Microscopy Services, Hatfield, PA, USA) and polymerized at 60 °C for 48 h. 200 nm sections were then acquired using a Leica EM UC6 ultramicrotome and added to six-well Teflon printed slides (Electron Microscopy Services). Slides were initially dried for 3–4.5 h on a slide warmer, then continued drying overnight at 45 °C to adhere tissue sections to the slide.

Antigen retrieval, blocking, and antibody incubations were then performed as follows, with the volume of each solution added being 100 µL/well. Antigen retrieval was initiated by incubation with 25 µg/mL proteinase K (Roche) in 1X PBS at 37 °C for 15 min. Following two washes with PBS pH 7.4, antigen retrieval was continued by three incubations in 0.5 M EDTA pH 8.0. After two PBS washes as above, autofluorescence was quenched by two incubations in 1 mg/mL $NaBH_4$. After another two washes, slides were placed in a humidity chamber for all remaining incubations. First, sections were incubated for 2 h in 4% normal goat serum in PBS pH 7.4 to inhibit non-specific antibody binding. Select wells were then incubated (overnight at 4 °C) with polyclonal rabbit anti-chicken collagen I antibodies (Millipore, Burlington, MA, USA, AB752P) diluted 1:40 in a primary dilution buffer (PDB = 0.1% bovine serum albumin/0.1% cold fish skin gelatin/0.5% Triton X-100/0.05% sodium azide/0.01 M PBS pH 7.3), chicken collagen-inhibited antibodies (same as above, at ~6 mg of lyophilized chicken collagen/mL in PDB, prepared separately), or in solely PBS pH 7.4 (for wells to serve as secondary-only controls). Following two washes

each with PBS pH 7.4/0.5% Tween 20 (PBS-T) then PBS pH 7.4, all wells were incubated for 2 h at RT with biotinylated goat anti-rabbit IgG H + L antibodies (Vector BA-1000) diluted 1:333 in a secondary dilution buffer (SDB = 0.01 M PBS pH 7.2/0.05% Tween 20). After four washes as above, wells were incubated for 1 h in the dark in fluorescein avidin D (FITC; Vector) diluted 1:1000 in SDB. After four final washes as above, slides were mounted with 5 µL/well of VectaShield H-1000 mounting medium. Cover slips were then applied and the slides were stored in the dark until imaging later the same day at 40X and 50 ms exposure using a Zeiss AxioSkop 2 Plus microscope with a connected AxioCam MRC5 camera. Digestion assays were also performed for select wells by incubation in 1 mg/mL collagenase A (Roche) in Dulbecco's PBS prior to antigen retrieval with proteinase K. Digestions were performed at 37 °C in a humidity chamber for 1 h (with changes each 20 min), after which slides were washed twice in PBS pH 7.4. Antigen retrieval then proceeded with proteinase K as described above.

3. Results

3.1. General Observations

Sediments within the iron trial chamber acquired a dark orange coloration within the first two weeks that was maintained for the remainder of the 90-day experiment. In the last few weeks of the experiment, the tip of the syringe for this trial frequently became blocked by precipitated iron oxides, briefly preventing the flow of waste solution into the waste beaker below. When this occurred, an autoclave-sterilized straight dissection pick was gently twisted within the syringe top to break up the clots of precipitated mineral and reestablish fluid flow. This was never necessary for the other three trials.

After completion of the trials, bones and sediment were emptied from each trial chamber and manually parsed from one another with separate, sterile, disposable scalpels. Contrary to expectations based on the results of Daniel and Chin [39], minimal sand was cemented to the external surfaces of the femur in the calcium carbonate trial. Bones from the deionized water control, calcium carbonate, and phosphate trials remained solid/hard to the touch and similar in color to when the experiment was begun (Figure 5). In sharp contrast, the femur from the iron trial was soft, pliable, and darkened in color. Yellow- and orange-stained sand was cemented over much of this bone, especially over its epiphyseal ends (Figure 5).

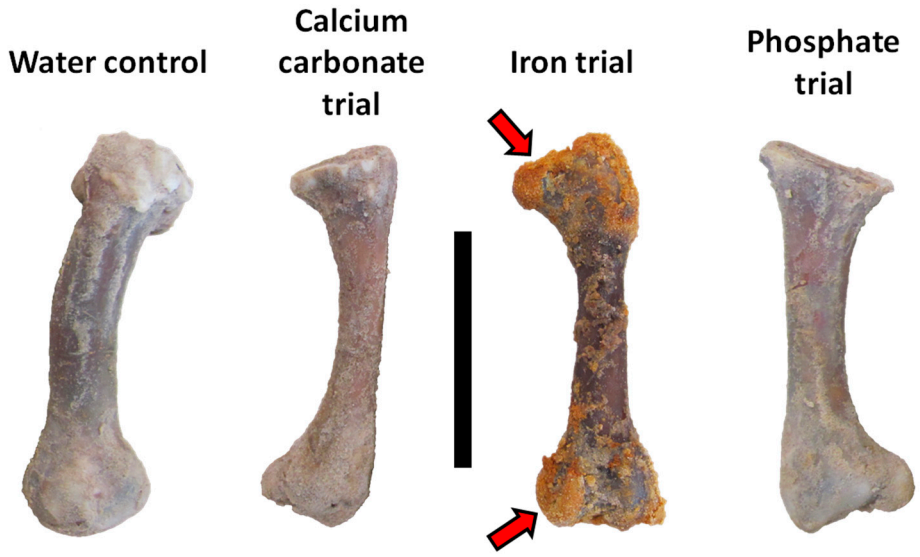

Figure 5. Chicken femora from each actualistic trial after completion of the experiment. Proximal ends are at top. Note sand adhered by an iron-oxide cement to the epiphyseal ends of the femur from the iron trial (red arrows). Scale bar equals 5 cm.

3.2. Histology

Histological integrity was generally well-preserved in all four trials. All four femora can be assigned a Histologic Index of 5 ("unaltered") according to the scale of Hedges et al. [85]. Osteons and osteocyte lacunae remained clearly visible in the thin section of each specimen. No bone sections exhibited any unequivocal evidence of microbial attack (i.e., Wedl tunneling, microscopic focal destructions [86]) or signs of recent bone mineral dissolution-reprecipitation induced by strains from burial or exposure to the various trial solutions (cf. [87]).

All four femora retained excellent preservation of original crystalline structure, as evidenced by retention of alternating dark and light bands (Figures 6B, 7B, 8B and 9B) and Maltese crosses (e.g., Figure 8B) under polarized light [32,88]. Maltese crosses are birefringence patterns that form as a product of hydroxyapatite crystal orientation; crystals that are aligned with their c axes parallel to the viewfinder block the passage of polarized light and appear dark, whereas crystals oriented in any other manner will allow the passage of light and appear bright. In an osteon in fresh bone, alternating layers of collagen fibrils and hydroxyapatite form an interference pattern that creates a cross of birefringence under polarized light which is centered around the Haversian canal at the center of the osteon [32]. Retention of these Maltese crosses in osteons of all trials indicates the mineral structure of the tissues has not been significantly altered.

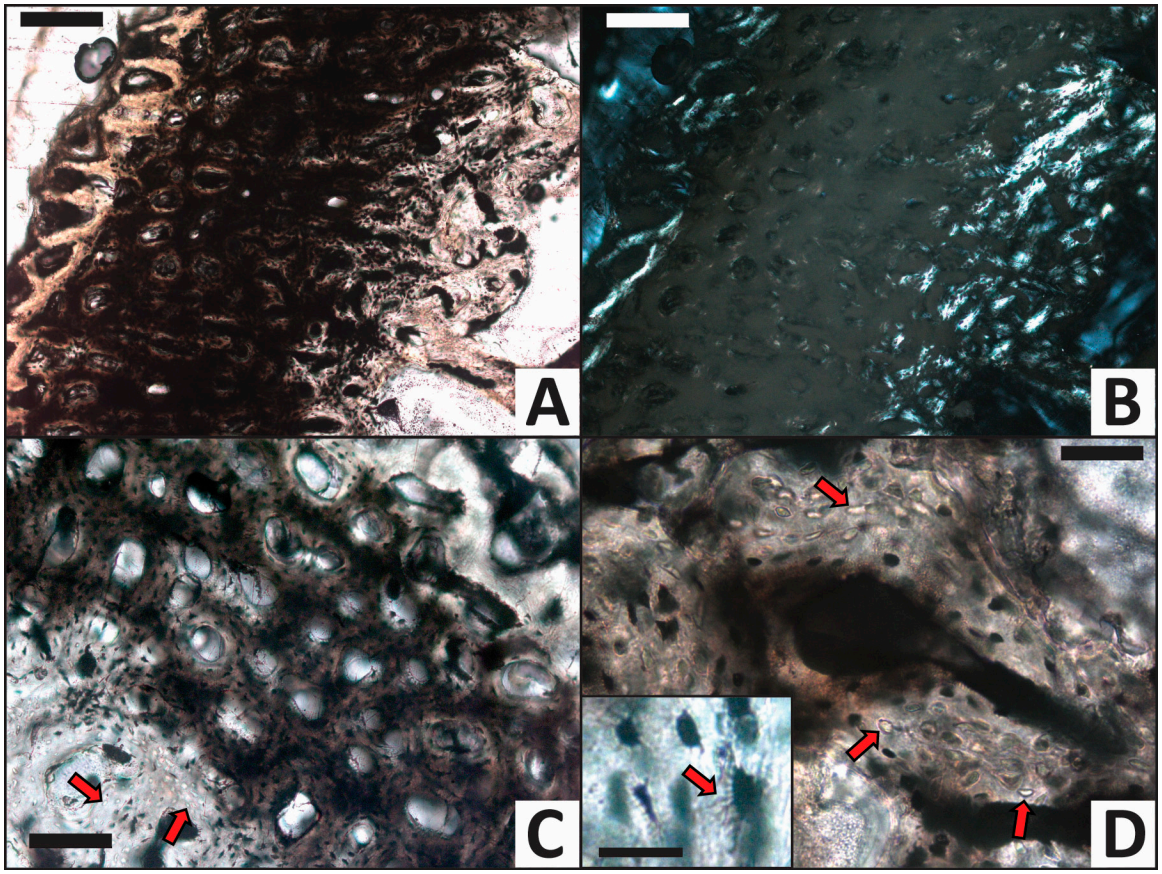

Figure 6. Histology of the femur from the water control trial after completion of the experiment. (**A**,**B**) Cross section of entire cortex in (**A**) transmitted light and (**B**) viewed with crossed polars. External cortex edge is at upper left, marrow cavity is at lower right. External and internal cortex are semitransparent but the middle cortex could not be ground to correct thickness; this region remains too thick and as a result appears opaque (dark brown) in transmitted light (**A**). This region appears a dark golden color under crossed polars (**B**). (**C**) Higher magnification of the cortex viewed by transmitted light, showing that Haversian canals remain open. Note that some osteocyte lacunae are

vacant (appear white) within the internal cortex (arrows). (**D**) Representative osteon in which some lacunae retain dark brown osteocytes while others are now empty (arrows). Inset displays well-preserved osteocytes which retain long, dark, intact filipodia (arrow). Scale bars for (**A**,**B**) equal 200 µm. Scale bar for (**C**) equals 100 µm. Scale bar for (**D**) equals 50 µm. Scale bar for inset in (**D**) equals 100 µm.

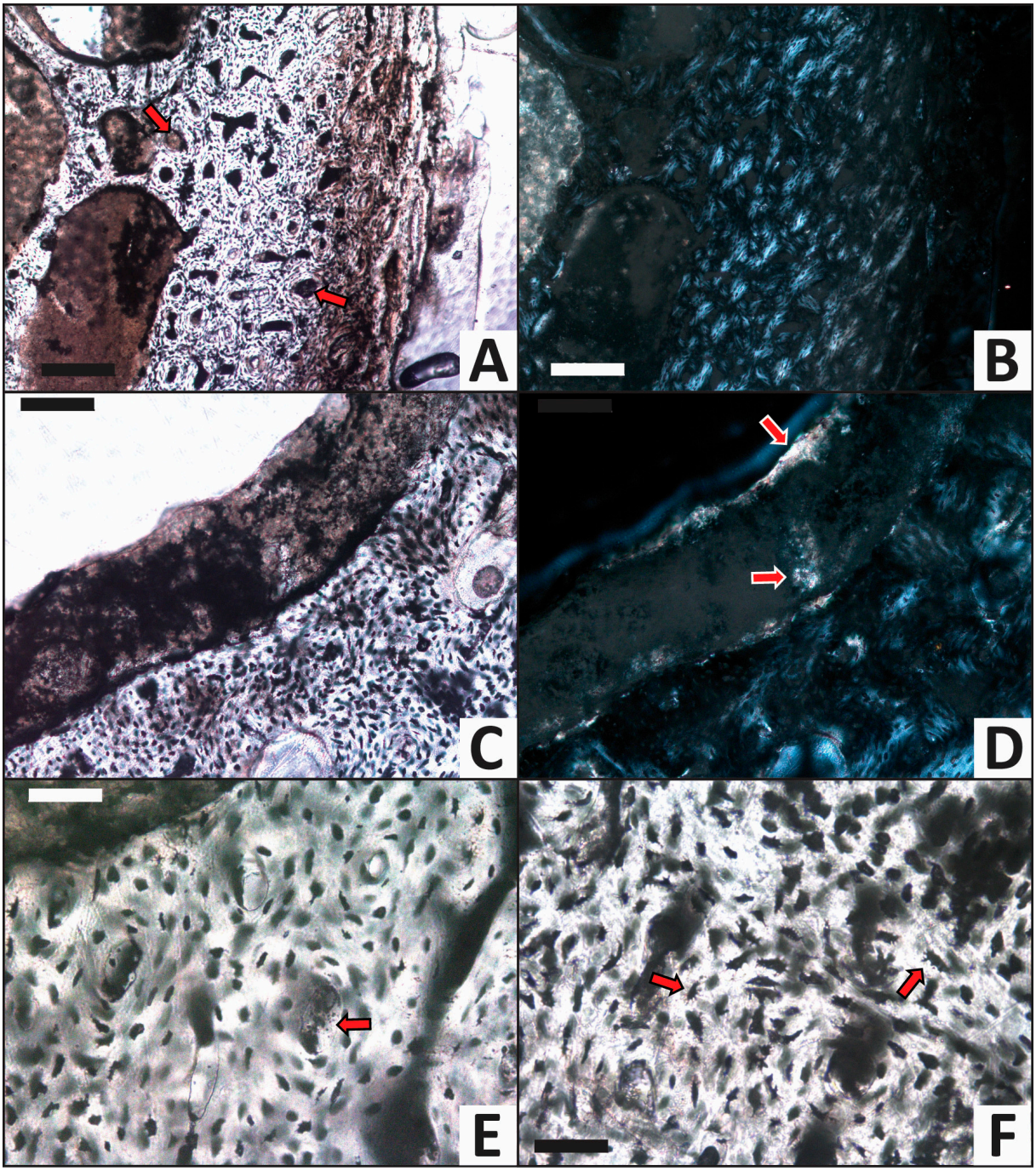

Figure 7. Histology of the femur from the calcium carbonate trial after completion of the experiment. (**A**,**B**) Cross section of entire cortex in (**A**) transmitted light and (**B**) viewed with crossed polars. External cortex edge is at right, marrow cavity is at left. Multiple Haversian canals are infilled by a tan-brown mineral precipitate (arrows). (**C**) Tan-brown, cryptocrystalline mineral precipitate lining the wall of a void in the marrow cavity. (**D**) Same as (**C**) viewed in cross-polarized light, showing

how patches of the mineral precipitate exhibit high order interference colors (arrows) characteristic of calcite. (**E**) A representative infilled Haversian canal (arrow) at higher magnification. Infilling mineral in this canal ranges from semi-translucent to tan-brown in color. (**F**) Representative well-preserved osteocytes which retain long, dark, intact filopodia (arrows). Scale bars for (**A**,**B**) equal 200 μm. Scale bars for (**C**,**D**) equal 100 μm. Scale bars for (**E**,**F**) equal 50 μm.

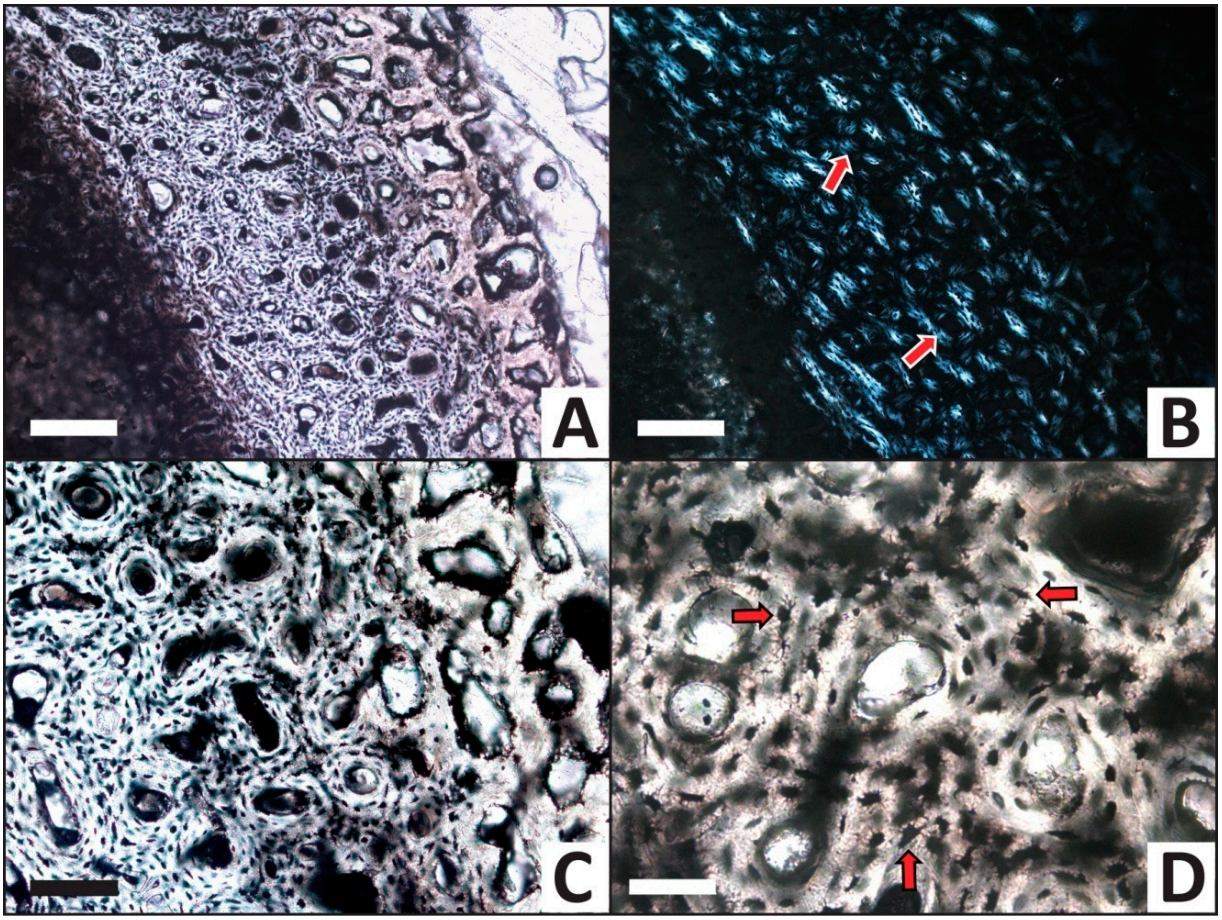

Figure 8. Histology of the femur from the phosphate trial after completion of the experiment. (**A**,**B**) Cross section of entire cortex in (**A**) transmitted light and (**B**) viewed with crossed polars. External cortex edge is at upper right, marrow cavity is at lower left. Excellent preservation of the tissue structure is evident under polarized light by presentation of Maltese crosses (arrows) by most osteons (see text for further discussion of these birefringence interference patterns). (**C**) Higher magnification of the external and middle cortex viewed by transmitted light, showing negligible alteration of bone microstructure and open Haversian canals. (**D**) Representative well-preserved osteocytes which retain long, dark, intact filopodia (arrows). Scale bars for (**A**,**B**) equal 200 μm. Scale bar for (**C**) equals 100 μm. Scale bar for (**D**) equals 50 μm.

Due to slight pliability of the femur from the water control trial, it was exceedingly difficult to grind/polish its thin section to even thickness, even within the scale of a single cortical wall. As a result, we were able to grind the internal cortex and outer cortical edge to optimal viewing thickness yet much of the middle cortex remains thicker than desired; this region consequently appears dark tan-brown under transmitted light (Figure 6A) and dark gold under polarized light (Figure 6B) rather than semitransparent. In order to not permanently lose the internal cortex and external cortical margin from the section, we did not conduct further grinding of the slide. Although fine structural details of the middle cortex consequently remain partially obscured, osteons are still clearly visible, as are osteocytes within lamellae around many osteons (e.g., Figure 6A,C). Haversian canals

remain open/unpermineralized (Figure 6C). Osteocytes remain present in many regions throughout the cortex, and they are typically dark red-brown in color, as in the calcium carbonate trial (see below). However, osteocytes are locally absent from lacunae in several small regions of the internal cortex, wherein they appear as bright, simple, ovoid entities (Figure 6D). Where osteocytes persist, they commonly retain visible filopodia (e.g., inset in Figure 6D). Filopodia were not encountered as frequently in this bone as in the femur from the calcium carbonate trial (see below).

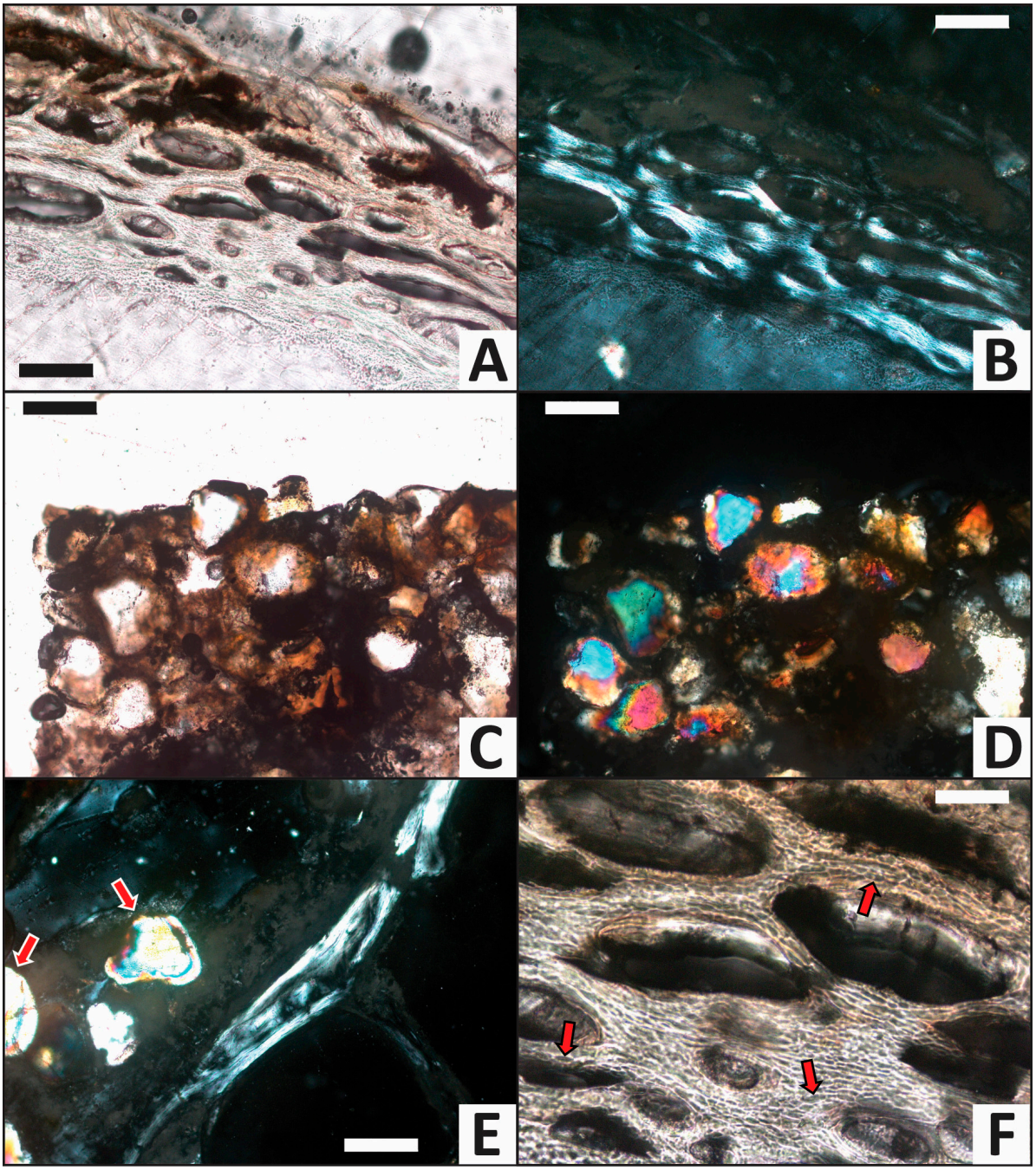

Figure 9. Histology of the femur from the iron trial after completion of the experiment. (**A**,**B**) Cross section of entire cortex in (**A**) transmitted light and (**B**) viewed with crossed polars. External cortex edge is at top, marrow cavity is at bottom. (**C**) Orange-brown, iron-rich mineral precipitate cementing sand grains together within a void in the marrow cavity. (**D**) Same as (**C**) viewed in cross-polarized light. Quartz sand grains exhibit moderate-order interference colors ranging from blue to green, pink,

orange, and yellow. (**E**) An iron-rich precipitate (gold-brown color) cementing sand grains (arrows) to one another and lining a strut of bone (the white, gray, and black linear feature passing from top right to bottom left) within the marrow cavity. (**F**) High magnification of the middle cortex, demonstrating universally-vacant osteocyte lacunae. Clearly visible examples are noted by arrows. Scale bars for (**A**,**B**) equal 100 µm. Scale bars for (**C**–**E**) equal 200 µm. Scale bar for (**F**) equals 50 µm.

A cryptocrystalline mineral precipitate frequently infills Haversian canals and partially infills medullary cavity voids in the femur from the calcium carbonate trial (Figure 7A–E). This precipitate also occasionally cements sand grains to walls within the internal medullary cavity. In transmitted light, these secondary mineral deposits appear semi-translucent to dark-tan in color (e.g., Figure 7C,E). Under crossed polars, the mineral linings generally appear golden-brown and locally include patches exhibiting bright, high-order interference colors (small regions of pastel colors; Figure 7D). Collectively, these optical characteristics identify the cryptocrystalline mineral precipitate to be calcite, as expected from the $CaCO_3$-supersaturated solution used in this trial. Osteocytes universally remain within lacunae, are dark red-brown in color, and consistently retain filopodial extensions from the cellular body (Figure 7F).

The femur from the phosphate trial appears essentially unaltered in histological structure (Figure 8A,B). Haversian canals frequently remain open (Figure 8C), hydroxyapatite crystal orientations are preserved (i.e., Maltese crosses are very common under crossed polars; Figure 8B), and osteocytes remain present throughout the entire section. As in the calcium carbonate trial (see above), osteocytes appear dark red-brown in color and retain clearly-visible, long filopodia (Figure 8D).

The femur from the iron trial exhibits the greatest alteration among the four trials (Figure 9A,B). A dark orange-brown mineral precipitate, identified as an iron oxyhydroxide mineral (most likely ferrihydrite and/or goethite) based on its optical characteristics and amorphous form, frequently lines and partially infills voids in the medullary cavity (Figure 9C–E). Subrounded sand grains are commonly cemented to one another by this new precipitate in the medullary cavity (e.g., Figure 9C,D). The sand grains, in contrast, commonly display a wide range of moderate-order interference colors (yellow, blue, pink, and purple) under cross-polarized light (e.g., Figure 9D,E), consistent with their identification as quartz. In contrast to all other trials, osteocyte lacunae are almost universally empty (Figure 9F). Osteocyte lacunae also appear proportionally larger and elongated (relative to the thickness of osteonal lamellae) in this femur than those from the other three trials.

3.3. ELISA

Collagen I was positively identified in all GuHCl extracts and most HCl extracts based on standard ELISA signal acceptance criteria (positive $\geq$ two times background levels; e.g., [89,90]). These results demonstrate that almost all extracted collagen I appears to be within the GuHCl extracts rather than the HCl extracts (Figure 10). In two of our three replicates, GuHCl extracts of the calcium carbonate trial reached saturation (3.0) more rapidly than did GuHCl extracts from the deionized water control. In the third replicate, GuHCl extracts of the water control reached saturation first. Saturation was normally reached in less than 90 min. That both the calcium carbonate and water control trials reached saturation so rapidly reflects negligible decay of collagen I in these trials. GuHCl extracts from the phosphate trials achieved slightly lower absorbance readings (~1.5–2.7) in 90 min than either the water control or the calcium carbonate trial. GuHCl extracts from the iron trial exhibited significantly lower absorbance than those from any other trials, generally yielding absorbance values ~0.7–1.8 in 90 min. In contrast, HCl extracts from the iron trial yielded greater absorbance readings than the HCl extracts from all three other trials, indicating that the initial demineralization in HCl more readily and rapidly freed collagen from the iron trial bone than from the bones from other trials; however, these readings still only reached ~0.1–0.3 in 90 min. Secondary-only and buffer blank control wells yielded no significant absorbance (Figure 10), respectively, confirming absence of

contaminants in the extraction buffers and lack of spurious binding of secondary antibodies to the plate.

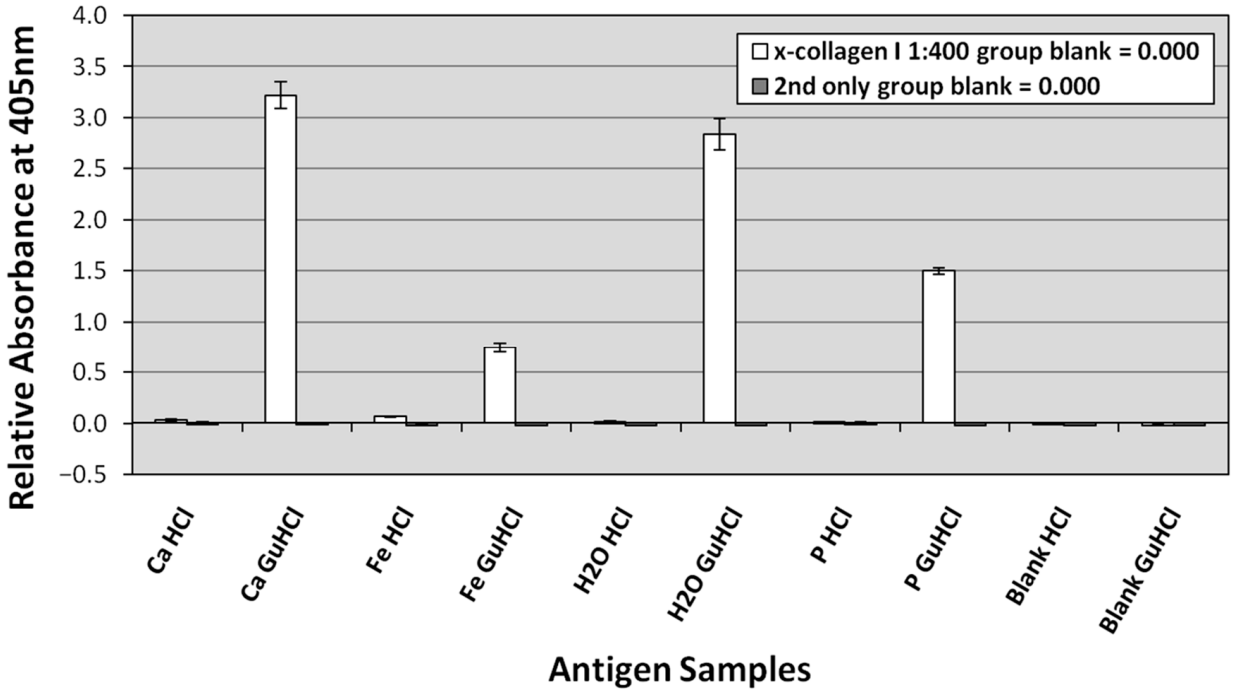

Figure 10. Representative ELISA testing bone HCl and GuHCl extracts from each actualistic trial against antibodies to chicken collagen I. The presented absorbance readings were taken at 405 nm at 150 min. Bone extracts were plated at 0.1 µg/well. Extraction blanks, testing laboratory reagents, are presented at right as 'Blank HCl' and 'Blank GuHCl'. The virtually indistinguishable dark gray bars to the right of the white bars present results from the secondary only controls (in which no primary antibodies were added).

3.4. Immunofluorescence

Collagen I was positively detected in all four femora (Figure 11A,E,I,M). In agreement with the ELISA results, fluorescent signal intensity was greatest for the femur from the water control trial (Figure 11A), of moderate intensity for the femur from the phosphate trial (Figure 11I), and weakest for the femur from the iron trial (Figure 11M). The femur from the calcium carbonate trial exhibited a fluorescent signal intermediate in intensity between those of the femora from the water control and phosphate trials (Figure 11E). Fluorescence was expressed throughout entire tissue sections of all four femora, consistent with collagen I comprising the majority of the proteinaceous matrix of bone tissues [91].

Secondary-only controls, in which anti-collagen antibodies were not added, present no fluorescence for all trials (Figure 11B,F,J,N), affirming a lack of non-specific binding by the secondary antibodies. Inhibition controls, in which primary antibodies were inhibited by incubation with purified chicken collagen prior to incubation with sample tissues, also exhibit no fluorescence (Figure 11C,G,K,O), confirming high specificity of the primary antibodies towards binding only to collagen I. Digestion controls, in which tissue sections were degraded by incubation for one hour with the enzyme collagenase, present dramatically reduced fluorescence in comparison to non-digested sections (Figure 11D,H,L,P). These results independently corroborate the presence of a protein with the tissue sections that is structurally consistent with collagen I (i.e., contains abundant Pro-X-Gly amino acid sequences that are rare in other proteins [92]).

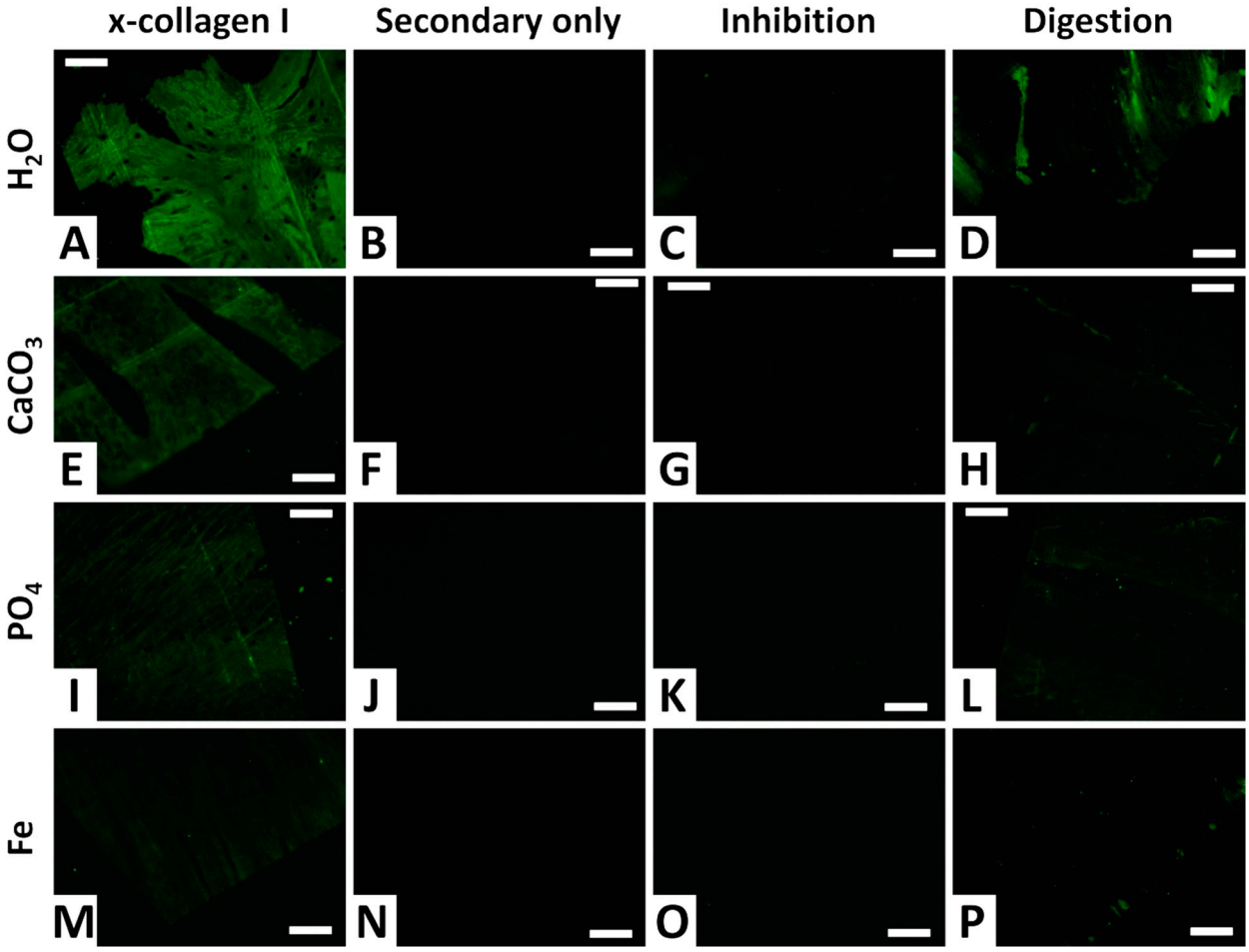

Figure 11. In situ immunofluorescence results showing the localization of collagen I in demineralized cortical fragments of chicken femora from each trial, alongside three different types of negative controls. All images show FITC-labeled antibody-antigen complexes under fluorescent light. (**A**–**D**) Water control trial. (**E**–**H**) Calcium carbonate trial. (**I**–**L**) Phosphate trial. (**M**–**P**) Iron trial. The first column (**A**,**E**,**I**,**M**) shows chicken femur tissue sections incubated with anti-chicken collagen I antibodies. The second column (**B**,**F**,**J**,**N**) shows secondary-only control sections that were not exposed to primary antibodies, to control for non-specific binding of secondary antibodies. The third column (**C**,**G**,**K**,**O**) shows sections exposed to anti-chicken collagen I antibodies that were first inhibited with chicken collagen (prior to incubation). The fourth column (**D**,**H**,**L**,**P**) shows sections digested with collagenase for 1 h prior to exposure to anti-collagen I antibodies. All section images were taken at 40X and 50 ms integration. All scale bars equal 50 μm.

4. Discussion

Our immunofluorescence and ELISA assays on GuHCl extracts positively identified collagen I remaining in the femur from each of the four trials (Figures 10 and 11), and results from these two immunoassays generally agree about the relative extent of decay of collagen I among the four trials: water control ≈ calcium carbonate < phosphate < iron (Table 1). The fact that collagen I accounts for ~90% of the organic fraction within bone [91] permits a rough approximation of the amount of collagen remaining in each trial's (GuHCl) extract. By this statistic, ~90 ng of the 100 ng of extract plated per well should be collagen I. Using the highest 150 min absorbance for reference (the calcium carbonate GuHCl absorbance in our third replicate, ~3.2) and including error bars of one standard deviation, percentage calculations indicate that our observed GuHCl absorbance values of 2.8–3.0, 1.5–2.7, and 0.7–1.8 reflect retention of 79–84 ng, 42–76 ng, and 20–51 ng collagen per 100 ng of extract from the water control, phosphate, and iron trial femora, respectively (compared to an

assumed 90 ng collagen/100 ng extract for the calcium carbonate trial femur). These findings suggest that approximately twice as much collagen was lost to decay in the iron trial than in the water control and calcium carbonate trials, and that the femur in the phosphate trial lost ~30% more collagen than the femora in those same two trials. Because all other variables were held constant among the trials (i.e., temperature, darkness, flow rate, taxonomic identity, bone density/microstructure type, and the same natural bacterial flora), these observed variations in collagen decay can be confidently attributed to exposure to simulated groundwater solutions of varied chemistry.

Table 1. Summary of bone attributes after completion of the experiment. Histological Index (HI) scores follow the ranking system of Hedges et al. [85]. Abbreviations: ELISA, enzyme-linked immunosorbent assay; IF, immunofluorescence.

Trial	HI after Experiment	Histologic Alterations	Relative ELISA Signal	Relative IF Signal
H_2O (control)	5	Some osteocytes lost to decay in internal cortex	High	High
$CaCO_3$	5	Common calcite infilling of Haversian canals, linings in medullary cavity	High	High
PO_4	5	Minimal signs of alteration, no mineral precipitate/linings	Moderate	Moderate
Fe	5	Common iron hydroxide infillings and linings, nearly all osteocytes lost to decay	Low	Low

Our four solutions differed in two aspects: the metal ion of enrichment and pH. The pH values of the solutions for the deionized water control (pH = 7), calcium carbonate (pH = 6.5), and phosphate (pH = 7) trials were purposefully adjusted to be circumneutral to simulate conditions in typical sedimentary environments known to be conducive to bone fossilization (e.g., fluviolacustrine settings), but iron chloride in the iron trial was allowed to hydrolyze ($Fe^{3+} + H_2O \rightarrow Fe[OH]^{2+} + H^+$) without pH counterbalancing, which ultimately made this solution highly acidic (pH = 2.2). The 10 mM $FeCl_3$ solution we used for the iron trial has been successfully used to promote rapid precipitation of iron oxyhdroxides (e.g., ferrihydrite) to simulate fossilization of bacteria [71] and leaves [93], but its low pH simulates diagenesis within an acidic, dysaerobic environment (e.g., swamp, marsh) that would be more likely to dissolve a bone than to preserve it as a fossil [31,94]. In fact, bones only tend to have high preservation potential in organic-poor, circumneutral to slightly-alkaline pH soils and sediments [31,95,96]. Thus, our iron trial modeled diagenesis within an environment that would not be conducive to bone fossilization, and, consequently, the considerable decay of collagen in the femur from this trial (Figures 10 and 11) is an expected result. Relatively greater decomposition of the femur in the iron trial is also evident by the softer post-experiment character of that bone compared to those from the other trials and the greater yield of collagen I within the HCl extract fraction from this bone than those from the other three trials (Figure 10).

Despite clear indications of partial dissolution of the femur in the iron trial (i.e., it was soft and pliable to the touch), precipitation of an amorphous, 'protective' iron cement occurred over much of the bone, especially over its epiphyseal ends (Figure 5). Greater development of iron cement/concretion over the epiphyseal ends of limb bones has also been previously reported from select nonavian dinosaur fossils (e.g., [97]). This phenomenon may be due to greater emission of iron-rich hemoglobin decay products from these cancellous tissue regions (than from regions of bones externally comprised of comparatively-denser compact cortical tissues).

At the molecular level, early-diagenetic encrustation of organic remains within precipitated iron oxyhydroxides has been hypothesized to elevate molecular preservation potential through: (1) physical shielding from exogenous microbes [98,99]; (2) inactivation of autolytic enzymes [71]; and/or (3) Fe-mediated inducement of (non-enzymatic) inter- and intramolecular crosslinking via Fenton and glycation reactions [69,70]. However, results from our iron trial definitively demonstrate that any 'protective' benefits from iron oxyhydroxide precipitation are insufficient to forestall molecular decay in highly-acidic diagenetic environments. Thus, in agreement with traditional perspectives [31,95], it is clear that the pH of the diagenetic environment constitutes an overarching control on bone fossilization—not only at the ultrastructural level, but also the molecular level.

Despite constant immersion under oxic conditions, the femur in the water control trial experienced surprisingly minimal collagen decay over the course of the experiment. This is particularly evident from its reaching saturation in ELISA within 90 min (Figure 10). One conceivable explanation for this result could be that our experiment was not run long enough for extensive microbial attack to take place; however, results from numerous published actualistic taphonomy experiments indicate that 90 days should be sufficient time to yield significant early-diagenetic changes (i.e., extensive decay, mineralization, or both; e.g., [38,39,69,71,93,100–106]). We therefore advance modest microbial attack as a more plausible, alternative explanation. This interpretation is supported by the rarity and spatial restriction of empty osteocyte lacunae to only within confined regions of the inner cortex (Figure 6C,D), as well as a complete absence of Wedl tunnels and microscopic focal destructions in the thin section of the femur from this trial (Figure 6). Although these findings imply only nominal microbial attack, microbial enzymes (autolytic, exogenic, or both) can still be confidently inferred to have been the primary agents of decay because the deionized water used in this trial was neutral in pH. Oxidation and hydrolysis [94,107] also probably contributed to decay, but strong ELISA and immunofluorescence signals for collagen in the femur from this control trial (Figures 10 and 11A) indicate that these processes did not cause significant decay of collagen over the duration of the experiment. Thus, collectively, results of the water control trial demonstrate that the duration of our experiment was sufficient to produce noticeable, but not necessarily substantial, decay (which was likely primarily driven by microbial attack).

The limited extent of observed microbial attack in the water control trial, and in our experiment in general, may also result inpart from our removal of the vast majority of soft tissues (i.e., muscles, ligaments) by dissection and degreasing prior to "burial" of the femora within the trial chambers. It should be noted, as discussed in the Methods, that removal of skin, muscle, and the majority of lipids was intentionally performed so that our results would provide insights specifically into the molecular-taphonomic trajectories of bones after skeletonization (the most common taphonomic pathway of bones in terrestrial ecosystems [46–49]). Vertebrate remains buried more immediately postmortem, and hence with a greater proportion of soft tissues such as muscles and skin still enshrouding them, could be expected to experience more significant microbial attack; presence of more of these water- and nutrient-rich tissues would be more likely to attract a greater abundance and diversity of endogenous (putrefactive) and exogenous (soil) microbial decomposers [108,109].

Lack of authigenic mineral precipitation in the phosphate trial indicates a phosphate concentration of twice maximum-reported natural abundance (9 mg/L [80]) was not high enough to induce inorganic nor bacterially-mediated precipitation (neither active nor passive). That inorganic precipitation did not occur is unsurprising (as the solution we utilized was prepared to well-below saturation), but it could be viewed surprising that bacterially-mediated precipitation did not occur. Lack of bacterially-mediated phosphate precipitation could be due to: (1) insufficient supply of phosphate in solution due to incomplete dissociation of H_3PO_4 and/or an insufficient supply of additional phosphate from the bone (because the pH was not acidic enough to cause significant hydroxyapatite dissolution); (2) insufficient presence of microbes around the bone to promote precipitation

of secondary mineral deposits; (3) the microbes present were incapable of inducing phosphate precipitation; or (4) a combination of these factors. Although each of these options is possible, the ubiquity of bacteria in modern environments, especially in moist settings at circumneutral pH [110], makes the second option above highly unlikely. We also view the third option, that the microbes present could not induce phosphate precipitation, to be implausible because the negatively-charged exopolysaccharides secreted by and encasing bacteria are known to easily and commonly bind a diverse array of metallic cations, which in turn frequently promotes mineral nucleation (e.g., [72,111–115]). This leaves option one above, insufficient availability of phosphate from solution and bone dissolution, as our favored explanation for the lack of phosphate precipitation in this trial. As a weak acid, phosphoric acid does not completely dissociate in water [116], and each of its three successive dissociations into phosphate release hydrogen ions (H^+) which could create brief, slightly-acidic conditions before the freed H^+ ions solvate with other anions: $H_3PO_4 \rightarrow H_2PO_4 + H^+$, $H_2PO_4 \rightarrow HPO_4 + H^+$, $HPO_4 \rightarrow PO_4 + H^+$ [117]. Although we did not track the pH of effluent solutions after they passed through the trial chambers, we speculate that gradual and incomplete phosphoric acid dissociation produced slightly acidic conditions within the phosphate trial chamber. The production of slightly acidic conditions in this trial could also reasonably explain how each of our immunoassays found the femur from the phosphate trial to have experienced an intermediate extent of collagen decay compared to the other trials (Figures 10 and 11I).

In contrast, permineralization with calcite clearly promoted stability of collagen within the femur in the calcium carbonate trial. For example, in two of our three ELISA replicates (e.g., Figure 10), absorbance readings for GuHCl extracts from this trial reached saturation even more rapidly than those from the femur from the deionized water control trial. Although histologic examination identified permineralization in the calcium carbonate trial to have been incomplete (Figure 7), this did not seem to be a limiting factor. Further, according to ELISA and immunofluorescence results (Figures 10 and 11), two of the three trials which did not produce extensive permineralization, namely the iron and phosphate trials, exhibited greater loss of collagen. Our results thus support prior predictions that (even partial) early-diagenetic permineralization can promote stabilization of not only the mineral component of bone, but also its soft tissues and their component biomolecules [15,118].

Collectively, our findings thus have several potentially-impactful implications to molecular paleontologists in regards to specimen selection. First, in agreement with prior inferences [15,118], we suggest that fossil bones exhibiting partial to complete early-diagenetic permineralization possess elevated molecular preservation potential, making them favorable candidates for paleomolecular analyses. In contrast, fossil bones which exhibit signs of having been exposed to acidic conditions during early diagenesis (e.g., surficial corrosion [119]) should be avoided when selecting specimens for paleomolecular analyses as they are likely to have experienced considerably greater biomolecular decay (in addition to loss of mineral; cf. [120]). Finally, our results imply that bones interpreted to have become encased in early-diagenetic concretions or rapidly-lithified sandstone may represent favorable specimens for paleomolecular studies.

5. Conclusions

Actualistic experiments offer a powerful means of investigating the roles of pore-fluid chemistry and other variables on the physical and chemical diagenesis of organic remains. In this study, we demonstrated that actualistic approaches can be equally informative toward understanding diagenesis at the molecular level. Specifically, by adapting methods developed by Carpenter [38] and Daniel and Chin [39] and integrating them with immunoassays for the first time, we were able to explore the influences of groundwater chemistry on collagen decay within bones encased in chambers simulating burial in a diverse range of diagenetic environments.

Our results yielded several novel and intriguing insights into biomolecular decay and stabilization. For example, results from our calcium carbonate trial identified that (even

partial) early permineralization can rapidly equilibrate a buried bone with its diagenetic environment and, by hindering microbial mobility, protect a portion of its soft tissues and biomolecules from microbial attack through protracted diagenesis. Similarly, results from our iron trial revealed that though iron enrichment in groundwater may facilitate early-diagenetic precipitation of 'protective' iron-hydroxide and/or iron-oxide cements/linings, these precipitates alone cannot prevent the dissolution of bone and decay of its biomolecules under highly-acidic diagenetic conditions.

Collectively, our findings demonstrate the uniquely-informative power of actualistic experimentation in the field of molecular paleontology. Critical variables ripe for further actualistic testing include sediment composition, the pH and flow rate of pore fluids, microbial community presence/absence (and composition), and sediment permeability, among others. For example, it would be intriguing to test whether the use of less porous and less permeable sediments (i.e., with a high fraction of clays) within this type of experiment might induce greater decay of collagen within bone due to the constrainment of decay fluids and microbes to within and around decaying remains (cf. [45]). Similarly, it would be intriguing to see if the use of more compositionally-immature sediments (i.e., a feldspathic litharenitic sand) induces greater decay as a result of the production of acidic conditions from gradual dissolution of feldspars and mafic grains. Such experiments hold great promise to advance understanding not only of the molecular taphonomy of collagen within bone, but also for DNA, carbohydrates, and other types of biomolecules in a wide array of animal and plant tissues. We therefore advocate for wider adoption of actualistic methods to clarify biomolecular decay and preservation pathways.

Author Contributions: Conceptualization, P.V.U. and K.J.L.; methodology, P.V.U.; formal analysis, P.V.U. and K.K.V.; investigation, P.V.U. and K.K.V.; resources, P.V.U. and K.J.L.; data curation, P.V.U.; writing—original draft preparation, P.V.U.; writing—review and editing, P.V.U. and K.K.V.; visualization, P.V.U.; project administration, P.V.U.; funding acquisition, P.V.U. All authors have read and agreed to the published version of the manuscript.

Funding: This research was funded by Drexel University and the National Science Foundation (NSF DGE 1002809, to P.V.U.).

Data Availability Statement: All data generated by this study are available in this manuscript.

Acknowledgments: This project would not have been possible without the support of Mary Schweitzer, who graciously opened her "Modern lab" at North Carolina State University to two of us (PVU and KKV) to conduct the ELISA and immunofluorescence assays for this project. We also thank Wenxia Zheng and Elena Schroeter for their advice and invaluable feedback while we performed the immunoassays presented herein. We are also grateful to James Spotila and Aleister Saunders at Drexel University for providing laboratory space for the duration of the project and for assistance in acquiring the supplies needed to construct the trial apparatuses, respectively.

Conflicts of Interest: The authors declare no conflict of interest.

References

1. Orlando, L.; Bonjean, D.; Bocherens, H.; Thenot, A.; Argant, A.; Otte, M.; Hanni, C. Ancient DNA and the population genetics of cave bears (*Ursus spelaeus*) through space and time. *Mol. Biol. Evol.* **2002**, *19*, 1920–1933. [CrossRef] [PubMed]
2. Asara, J.M.; Schweitzer, M.H.; Freimark, L.M.; Phillips, M.; Cantley, L.C. Protein sequences from mastodon and *Tyrannosaurus rex* revealed by mass spectrometry. *Science* **2007**, *316*, 280–285. [CrossRef] [PubMed]
3. Schweitzer, M.H.; Suo, Z.; Avci, R.; Asara, J.M.; Allen, M.A.; Arce, F.T.; Horner, J.R. Analyses of soft tissue from *Tyrannosaurus rex* suggest the presence of protein. *Science* **2007**, *316*, 277–280. [CrossRef]
4. Schweitzer, M.H.; Zheng, W.; Organ, C.L.; Avci, R.; Suo, Z.; Freimark, L.M.; Lebleu, V.S.; Duncan, M.B.; Vander Heiden, M.G.; Neveu, J.M.; et al. Biomolecular characterization and protein sequences of the Campanian hadrosaur *B. canadensis*. *Science* **2009**, *324*, 626–631. [CrossRef] [PubMed]
5. Schweitzer, M.H.; Zheng, W.; Cleland, T.P.; Bern, M. Molecular analyses of dinosaur osteocytes support the presence of endogenous molecules. *Bone* **2013**, *52*, 414–423. [CrossRef]
6. Cappellini, E.; Jensen, L.J.; Szklarczyk, D.; Ginolhac, A.; da Fonseca, R.A.R.; Stafford, T.W., Jr.; Holen, S.R.; Collins, M.J.; Orlando, L.; Willerslev, E.; et al. Proteomic analysis of a Pleistocene mammoth femur reveals more than one hundred ancient bone proteins. *J. Proteome Res.* **2012**, *11*, 917–926. [CrossRef]

7. Lindgren, J.; Uvdal, P.; Engdahl, A.; Lee, A.H.; Alwmark, C.; Bergquist, K.-E.; Nilsson, E.; Ekström, P.; Rasmussen, M.; Douglas, D.A.; et al. Microspectroscopic evidence of Cretaceous bone proteins. *PLoS ONE* **2011**, *6*, e19445. [CrossRef]
8. Hofreiter, M.; Collins, M.; Stewart, J.R. Ancient biomolecules in Quaternary palaeoecology. *Quat. Sci. Rev.* **2012**, *33*, 1–13. [CrossRef]
9. Cleland, T.P.; Schroeter, E.R.; Zamdborg, L.; Zheng, W.; Lee, J.E.; Tran, J.C.; Bern, M.; Duncan, M.B.; Lebleu, V.S.; Ahlf, D.R.; et al. Mass spectrometry and antibody-based characterization of blood vessels from *Brachylophosaurus canadensis*. *J. Proteome Res.* **2015**, *14*, 5252–5262. [CrossRef]
10. Cleland, T.P.; Schroeter, E.R.; Feranec, R.S.; Vashishth, D. Peptide sequences from the first *Castoroides ohioensis* skull and the utility of old museum collections for palaeoproteomics. *Proc. R. Soc. B* **2016**, *283*, 20160593. [CrossRef]
11. Schroeter, E.R.; DeHart, C.J.; Cleland, T.P.; Zheng, W.; Thomas, P.M.; Kelleher, N.L.; Bern, M.; Schweitzer, M.H. Expansion for the *Brachylophosaurus canadensis* collagen I sequence and additional evidence of the preservation of Cretaceous protein. *J. Proteome Res.* **2017**, *16*, 920–932. [CrossRef] [PubMed]
12. Schroeter, E.R.; Ullmann, P.V.; Zheng, W.; Schweitzer, M.H.; Lacovara, K.J. Soft-tissue, rare earth element, and molecular analyses of *Dreadnoughtus schrani*, an exceptionally complete titanosaur from Argentina. *Biology* **2022**, *11*, 1158. [CrossRef] [PubMed]
13. Bobrovskiy, I.; Hope, J.M.; Ivantsov, A.; Nettersheim, B.J.; Hallmann, C.; Brocks, J.J. Ancient steroids establish the Ediacaran fossil *Dickinsonia* as one of the earliest animals. *Science* **2018**, *361*, 1246–1249. [CrossRef]
14. Barnett, R.; Westbury, M.V.; Sandoval-Velasco, M.; Vieira, F.G.; Jeon, S.; Zazula, G.; Martin, M.D.; Ho, S.Y.W.; Mather, N.; Gopalakrishnan, S.; et al. Genomic adaptations and evolutionary history of the extinct scimitar-toothed cat. *Homotherium latidens*. *Curr. Biol.* **2020**, *30*, 5018–5025. [CrossRef]
15. Ullmann, P.V.; Voegele, K.K.; Grandstaff, D.E.; Ash, R.D.; Zheng, W.; Schroeter, E.R.; Schweitzer, M.H.; Lacovara, K.J. Molecular tests support the viability of rare earth elements as proxies for fossil biomolecule preservation. *Sci. Rep.* **2020**, *10*, 15566. [CrossRef]
16. Voegele, K.K.; Ullmann, P.V.; Boles, Z.M.; Schroeter, E.R.; Zheng, W.; Schweitzer, M.H.; Lacovara, K.J. Soft tissue and biomolecular preservation in vertebrate fossils from glauconitic, shallow marine sediments of the Hornerstown Formation, Edelman Fossil Park, New Jersey. *Biology* **2022**, *11*, 1161. [CrossRef] [PubMed]
17. Buckley, M.; Collins, M.; Thomas-Oates, J.; Wilson, J.C. Species identification by analysis of bone collagen using matrix-assisted laser desorption/ionisation time-of-flight mass spectrometry. *Rapid Commun. Mass Spectrom.* **2009**, *23*, 3843–3854. [CrossRef]
18. Buckley, M.; Larkin, N.; Collins, M. Mammoth and *Mastodon* collagen sequences; survival and utility. *Geochim. Cosmochim. Acta* **2011**, *75*, 2007–2016. [CrossRef]
19. Organ, C.L.; Schweitzer, M.H.; Zheng, W.; Freimark, L.M.; Cantley, L.C.; Asara, J.M. Molecular phylogenetics of *Mastodon* and *Tyrannosaurus rex*. *Science* **2008**, *320*, 499. [CrossRef]
20. Welker, F.; Collins, M.J.; Thomas, J.A.; Wadsley, M.; Brace, S.; Cappellini, E.; Turvey, S.T.; Requero, M.; Gelfo, J.N.; Kramarz, A.; et al. Ancient proteins resolve the evolutionary history of Darwin's South American ungulates. *Nature* **2015**, *522*, 81–84. [CrossRef]
21. Cappellini, E.; Welker, F.; Pandolfi, L.; Ramos-Madrigal, J.; Samodova, D.; Rüther, P.L.; Fotakis, A.K.; Lyon, D.; Moreno-Mayar, J.V.; Bukhsianidze, M.; et al. Early Pleistocene enamel proteome from Dmanis resolves *Stephanorhinus* phylogeny. *Nature* **2019**, *574*, 103–107. [CrossRef] [PubMed]
22. Buckley, M.; Recabarren, O.P.; Lawless, C.; García, N.; Pino, M. A molecular phylogeny of the extinct South American gomphothere through collagen sequence analysis. *Quat. Sci. Rev.* **2019**, *224*, 105882. [CrossRef]
23. Buckley, M.; Harvey, V.L.; Orihuela, J.; Mychajliw, A.M.; Keating, J.N.; Milan, J.N.A.; Lawless, C.; Chamberlain, A.T.; Egerton, V.M.; Manning, P.L. Collagen sequence analysis reveals evolutionary history of extinct West Indies *Nesophontes* (island-shrews). *Mol. Biol. Evol.* **2020**, *37*, 2931–2943. [CrossRef] [PubMed]
24. Presslee, S.; Slater, G.J.; Pujos, F.; Forasiepi, A.M.; Fischer, R.; Molloy, K.; Mackie, M.; Olsen, J.V.; Kramarz, A.; Taglioretti, M.; et al. Palaeoproteomics resolves sloth relationships. *Nat. Ecol. Evol.* **2019**, *3*, 1121–1130. [CrossRef] [PubMed]
25. Orlando, L.; Ginolhac, A.; Zhang, G.; Froese, D.; Albrechtsen, A.; Stiller, M.; Schubert, M.; Cappellini, E.; Petersen, B.; Moltke, I.; et al. Recalibrating *Equus* evolution using the genome sequence of an early Middle Pleistocene horse. *Nature* **2013**, *499*, 74–78. [CrossRef] [PubMed]
26. Pääbo, S.; Poinar, H.; Serre, D.; Jaenicke-Després, V.; Hebler, J.; Rohland, N.; Kuch, M.; Krause, J.; Vigilant, L.; Hofreiter, M. Genetic analyses from ancient DNA. *Annu. Rev. Genet.* **2004**, *38*, 645–679. [CrossRef] [PubMed]
27. Rogaev, E.I.; Moliaka, Y.K.; Malyarchuk, B.A.; Kondrashov, F.A.; Derenko, M.V.; Chumakov, I.; Grigorenko, A.P. Complete mitochondrial genome and phylogeny of Pleistocene mammoth *Mammuthus primigenius*. *PLoS Biol.* **2006**, *4*, e73. [CrossRef] [PubMed]
28. van der Valk, T.; Pečnerová, P.; Díez-del-Molino, D.; Bergström, A.; Oppenheimer, J.; Hartmann, S.; Xenikoudakis, G.; Thomas, J.A.; Dehasque, M.; Sağlican, E.; et al. Million-year-old DNA sheds light on the genomic history of mammoths. *Nature* **2021**, *591*, 265–269. [CrossRef]
29. Pan, Y.; Zheng, W.; Sawyer, R.H.; Pennington, M.W.; Zheng, X.; Wang, X.; Wang, M.; Hu, L.; O'Connor, J.; Zhao, T.; et al. The molecular evolution of feathers with direct evidence from fossils. *Proc. Natl Acad. Sci. USA* **2019**, *116*, 3018–3023. [CrossRef]
30. Zimmerman, E.A.; Schaible, E.; Gludovatz, B.; Schmidt, F.N.; Riedel, C.; Krause, M.; Vettorazzi, E.; Acevedo, C.; Hahn, M.; Püshcel, K.; et al. Intrinsic mechanical behavior of femoral cortical bone in young, osteoporotic and bisphosphonate-treated individuals in low- and high energy fracture conditions. *Sci. Rep.* **2016**, *6*, 21072. [CrossRef]

31. Behrensmeyer, A.K.; Hook, R.W.; Badgley, C.E.; Boy, J.A.; Chapman, R.E.; Dodson, P.; Gastaldo, R.A.; Graham, R.W.; Martin, L.D.; Olsen, P.E.; et al. Paleoenvironmental contexts and taphonomic modes. In *Evolutionary Paleoecology of Terrestrial Plants and Animals*; Behrensmeyer, A.K., Damuth, J.D., DiMichele, W.A., Potts, R., Sues, H.-D., Wing, S.L., Eds.; Chicago University Press: Chicago, IL, USA, 1992; pp. 15–136.
32. Hubert, J.F.; Panish, P.T.; Chure, D.J.; Prostak, K.S. Chemistry, microstructure, petrology, and diagenetic model of Jurassic dinosaur bones, Dinosaur National Monument, Utah. *J. Sediment. Res.* **1996**, *66*, 531–547.
33. Berna, F.; Matthews, A.; Weiner, S. Solubilities of bone mineral from archaeological sites: The recrystallization window. *J. Anthropol. Sci.* **2004**, *31*, 867–882. [CrossRef]
34. Tütken, T.; Vennemann, T.W.; Pfretzschner, H.-U. Early diagenesis of bone and tooth apatite in fluvial and marine settings: Constraints from combined oxygen isotope, nitrogen and REE analysis. *Palaeogeogr. Palaeocl.* **2008**, *266*, 254–268. [CrossRef]
35. Kowal-Linka, M.; Jochum, K.P.; Surmik, D. LA-ICP-MS analysis of rare earth elements in marine reptile bones from the Middle Triassic bonebed (Upper Silesia, S Poland): Impact of long-lasting diagenesis, and factors controlling the uptake. *Chem. Geol.* **2014**, *363*, 213–228. [CrossRef]
36. Kowal-Linka, M.; Jochum, K.P. Variability of trace element uptake in marine reptile bones from three Triassic sites (S Poland): Influence of diagenetic processes on the host rock and significance of the applied methodology. *Chem. Geol.* **2015**, *397*, 1–13. [CrossRef]
37. Kowalewski, M.; Labarbera, M. Actualistic taphonomy: Death, decay, and disintegration in contemporary settings. *PALAIOS* **2004**, *19*, 423–427. [CrossRef]
38. Carpenter, K. Experimental investigation of the role of bacteria in bone fossilization. *Neues Jahrb. Geol. Paläontologie Mon.* **2005**, *2*, 83–94. [CrossRef]
39. Daniel, J.C.; Chin, K. The role of bacterially mediated precipitation in the permineralization of bone. *PALAIOS* **2010**, *25*, 507–516. [CrossRef]
40. Varricchio, D.J.; Jackson, F.J.; Scherzer, B.; Shelton, J. Don't have a cow, man! It's only actualistic taphonomy on the Yellowstone River of Montana. *J. Vert. Paleo.* **2005**, *25* (Suppl. 3), 126A.
41. Voorhies, M.R. *Taphonomy and Population Dynamics of an Early Pliocene Vertebrate Fauna, Knox County, Nebraska*; Contributions to Geology Special Paper No. 1; University of Wyoming: Laramie, WY, USA, 1969; Volume 1, pp. 1–69.
42. Aslan, A.; Behrensmeyer, A.K. Taphonomy and time resolution of bone assemblages in a contemporary fluvial system: The East Fork River, Wyoming. *PALAIOS* **1996**, *11*, 411–421. [CrossRef]
43. Kohn, M.J.; Moses, R.J. Trace element diffusivities in bone rule out simple diffusive uptake during fossilization but explain in vivo uptake and release. *Proc. Natl. Acad. Sci. USA* **2013**, *110*, 419–424. [CrossRef] [PubMed]
44. Krajcarz, M.T. Alteration of the metal content in animal bones after 2.5-year experimental exposure to sediments. *Achaeol. Anthropol. Sci.* **2019**, *11*, 361–372. [CrossRef]
45. Peterson, J.E.; Lenczewski, M.E.; Clawson, S.R.; Warnock, J.P. Role of sediment size and biostratinomy on the development of biofilms in recent avian vertebrate remains. *Front. Earth Sci.* **2017**, *5*, 30. [CrossRef]
46. Behrensmeyer, A.K. Taphonomic and ecologic information from bone weathering. *Paleobiology* **1978**, *4*, 150–162. [CrossRef]
47. Brett, C.E.; Baird, G.C. Comparative taphonomy: A key to paleoenvironmental interpretation based on fossil preservation. *PALAIOS* **1986**, *1*, 207–227. [CrossRef]
48. Madgwick, R.; Mulville, J. Investigating variation in the prevalence of weathering in faunal assemblages in the UK: A multivariate statistical approach. *Int. J. Osteoarchaeol.* **2011**, *22*, 509–522. [CrossRef]
49. Pokines, J.T.; Faillace, K.; Berger, J.; Pirtle, D.; Sharpe, M.; Curtis, A.; Lombardi, K.; Admans, J. The effects of repeated wet-dry cycles as a component of bone weathering. *J. Archaeol. Sci. Rep.* **2018**, *17*, 433–441. [CrossRef]
50. Schroeter, E.R.; DeHart, C.J.; Schweitzer, M.H.; Thomas, P.M.; Keller, N.L. Bone protein "extractomics": Comparing the efficiency of bone protein extractions of *Gallus gallus* in tandem mass spectrometry. *PeerJ* **2016**, *4*, e2603. [CrossRef] [PubMed]
51. Ayars, J.; Gao, Y. Atmospheric nitrogen deposition to the Mullica River-Great Bay Estuary. *Mar. Environ. Res.* **2007**, *64*, 590–600. [CrossRef]
52. Iannuzzi, T.J.; Armstrong, T.N.; Thelen, J.B.; Ludwig, D.F.; Firstenberg, C.E. Characterization of chemical contamination in shallow-water estuarine habitats of an industrialized river. Part I: Organic compounds. *Soil Sediment Contam.* **2005**, *14*, 13–33. [CrossRef]
53. Armstrong, T.N.; Iannuzzi, T.J.; Thelen, J.B.; Ludwig, D.F.; Firstenberg, C.E. Characterization of chemical contamination in shallow-water estuarine habitats of an industrialized river. Part II: Metals. *Soil Sediment Contam.* **2005**, *14*, 35–52. [CrossRef]
54. Leduc, M.; Kasra, R.; van Heijenoort, J. Induction and control of the autolytic system of *Escherichia coli*. *J. Bacteriol.* **1982**, *152*, 26–34. [CrossRef] [PubMed]
55. Coolbear, T.; Whittaker, J.M.; Daniel, R.M. The effect of metal ions on the activity and thermostability of the extracellular proteinase from a thermophilic *Bacillus*, strain EA.1. *Biochem. J.* **1992**, *287*, 367–374. [CrossRef] [PubMed]
56. Francillon-Vieillot, H.; de Buffrénil, V.; Castanet, J.; Géraudie, J.; Meunier, F.J.; Sire, J.Y.; Zylberberg, L.; de Ricqlès, A. Microstructure and mineralization of vertebrate skeletal tissues. In *Skeletal Biomineralization Patterns, Processes and Evolutionary Trends*; Carter, J.G., Ed.; Van Nostrand Reinhold: New York, NY, USA, 1990; pp. 471–547.

57. Ehrlich, H.L. How microbes influence mineral growth and dissolution. *Chem. Geol.* **1996**, *132*, 5–9. [CrossRef]
58. Gadd, G.M. Metals, minerals and microbes: Geomicrobiology and bioremediation. *Microbiology* **2010**, *156*, 609–643. [CrossRef] [PubMed]
59. Wings, O. Authigenic minerals in fossil bones from the Mesozoic of England: Poor correlation with depositional environments. *Palaeogeog. Palaeocl.* **2004**, *204*, 15–32. [CrossRef]
60. Rogoz, A.; Sawlowicz, Z.; Wojtal, P. Diagenetic history of Woolly Mammoth (*Mammuthus primigenius*) skeletal remains from the archaeological site Cracow Spadzista Street (B), southern Poland. *PALAIOS* **2012**, *27*, 541–549. [CrossRef]
61. Bodzioch, A. Idealized model of mineral infillings in bones of fossil freshwater animals, on the example of Late Triassic metoposaurs from Krasiejów (Poland). *Austin J. Earth Sci.* **2015**, *2*, 1008.
62. Coto, B.; Martos, C.; Peña, J.L.; Rodríguez, R.; Pastor, G. Effects in the solubility of $CaCO_3$: Experimental study and model description. *Fluid Phase Equilibr.* **2012**, *324*, 1–7. [CrossRef]
63. Livingstone, D.A. Chemical composition of rivers and lakes. In *Data of Geochemistry*; Fleischer, M., Ed.; USGS: Washington, DC, USA, 1963; pp. 1–64.
64. Chapelle, F.H.; Lovley, D.R. Competitive exclusion of sulfate reduction by Fe(III)-reducing bacteria: A mechanism for producing discrete zones of high-iron ground water. *Groundwater* **1992**, *30*, 29–36. [CrossRef]
65. Previtera, E.; Mancuso, A.C.; de la Fuente, M.S.; Sánchez, E.S. Diagenetic analyses of tetrapod from the Upper Triassic, Puesto Viejo Group, Argentina. *Andean Geol.* **2016**, *43*, 197–214. [CrossRef]
66. Previtera, E. Bone microstructure and diagenesis of saurischian dinosaurs from the Upper Cretaceous (Neuquén Group), Argentina. *Andean Geol.* **2017**, *44*, 39–58. [CrossRef]
67. Ullmann, P.V.; Pandya, S.H.; Nellermoe, R. Patterns of soft tissue and cellular preservation in relation to fossil bone microstructure and overburden depth at the Standing Rock Hadrosaur Site, Maastrichtian Hell Creek Formation, South Dakota, USA. *Cretaceous Res.* **2019**, *99*, 1–13. [CrossRef]
68. Schweitzer, M.H.; Wittmeyer, J.L.; Horner, J.R. Soft tissue and cellular preservation in vertebrate skeletal elements from the Cretaceous to the present. *Proc. R. Soc. B* **2007**, *274*, 183–197. [CrossRef] [PubMed]
69. Schweitzer, M.H.; Zheng, W.; Cleland, T.P.; Goodwin, M.B.; Boatman, E.; Theil, E.; Marcus, M.A.; Fakra, S.C. A role for iron and oxygen chemistry in preserving soft tissues, cells and molecules from deep time. *Proc. R. Soc. B* **2014**, *281*, 20132741. [CrossRef]
70. Boatman, E.M.; Goodwin, M.B.; Holman, H.-Y.N.; Fakra, S.; Zheng, W.; Gronsky, R.; Schweitzer, M.H. Mechanisms of soft tissue and protein preservation in *Tyrannosaurus rex*. *Sci. Rep.* **2019**, *9*, 15678. [CrossRef]
71. Ferris, F.G.; Fyfe, W.S.; Beveridge, T.J. Metallic ion binding by *Bacillus subtilis*: Implications for the fossilization of microorganisms. *Geology* **1988**, *16*, 149–152. [CrossRef]
72. Hirschler, A.; Lucas, J.; Hubert, J.-C. Apatite genesis: A biologically induced or biologically controlled mineral formation process? *Geomicrobiol. J.* **1990**, *7*, 47–57. [CrossRef]
73. Prevot, L.; Lucas, J. Phosphate. In *Paleobiology: A Synthesis*; Briggs, D.E.G., Crowther, P.R., Eds.; Blackwell Scientific Publications: Oxford, UK, 1990; pp. 256–257.
74. Martill, D.M. Preservation of fish in the Cretaceous Santana Formation of Brazil. *Paleontology* **1988**, *32*, 1–18.
75. Martill, D.M. Macromolecular resolution of fossilized muscle tissue from an elopomorph fish. *Nature* **1990**, *346*, 171–172. [CrossRef]
76. Kellner, A.W.A. Fossilized theropod soft tissue. *Nature* **1996**, *379*, 32. [CrossRef]
77. Briggs, D.E.G.; Wilby, P.R.; Perez-Moreno, B.P.; Sanz, J.L.; Fregenal-Martinez, M. The mineralization of dinosaur soft tissue in the Lower Cretaceous of Las Hoyas, Spain. *J. Geol. Soc.* **1997**, *154*, 587. [CrossRef]
78. Briggs, D.E.G. The role of decay and mineralization in the preservation of soft-bodied fossils. *Annu. Rev. Earth Pl. Sc.* **2003**, *31*, 275–301. [CrossRef]
79. Zhu, M.; Babcock, L.E.; Steiner, M. Fossilization modes in the Chengjiang Lagerstatte (Cambrian of China): Testing the roles of organic preservation and diagenetic alteration in exceptional preservation. *Palaeogeogr. Palaeocl.* **2005**, *220*, 31–46. [CrossRef]
80. Sheldon, R.P. Ancient marine phosphates. *Annu. Rev. Earth Pl. Sc.* **1981**, *9*, 251–284. [CrossRef]
81. McNamara, M.E.; Orr, P.J.; Kearns, S.L.; Alcalá, L.; Anadón, P.; Peñalver-Mollá, E. High-fidelity organic preservation of bone marrow in ca. 10 Ma amphibians. *Geology* **2006**, *34*, 641–644. [CrossRef]
82. Lamm, E.-T. Preparation and sectioning of specimens. In *Bone Histology of Fossil Tetrapods*; Padian, K., Lamm, E.-T., Eds.; University of California Press: Berkeley, CA, USA, 2013; pp. 55–160.
83. Schroeter, E.A.R. The Morphology, Histology, and Molecular Preservation of an Exceptionally Complete Titanosaur from Southernmost Patagonia. Ph.D. Thesis, Drexel University, Philadelphia, PA, USA, 2013.
84. Zheng, W.; Schweitzer, M.H. Chemical analyses of fossil bone. In *Forensic Microscopy for Skeletal Tissues: Methods and Protocols*; Bell, L., Ed.; Humana Press: New York, NY, USA, 2012; pp. 153–172.
85. Hedges, R.E.M.; Millard, A.R.; Pike, A.W.G. Measurements and relationships of diagenetic alteration of bone from three archaeological sites. *J. Archaeol. Sci.* **1995**, *22*, 201–209. [CrossRef]
86. Jans, M.M.E. Microbial bioerosion of bone—A review. In *Current Developments in Bioerosion*; Wisshak, M., Tapanila, L., Eds.; Springer: Berlin/Heidelberg, Germany, 2008; pp. 397–413.

87. Putra, R.U.; Basri, H.; Prakoso, A.T.; Chandra, H.; Ammarullah, M.I.; Akbar, I.; Syahrom, A.; Kamarul, T. Level of activity changes increases the fatigue life of the porous magnesium scaffold, as observed in dynamic immersion tests, over time. *Sustainability* **2023**, *15*, 823. [CrossRef]
88. Jans, M.M.E.; Kars, H.; Nielsen-Marsh, C.M.; Smith, C.I.; Nord, A.G.; Arthur, P.; Earl, N. In situ preservation of archaeological bone: A histological study within a multidisciplinary approach. *Archaeometry* **2002**, *44*, 343–352. [CrossRef]
89. Ostlund, E.N.; Crom, R.L.; Pedersen, D.D.; Johnson, D.J.; Williams, W.O.; Schmitt, B.J. Equine West Nile encephalitis, United States. *Emerg. Infect. Dis.* **2001**, *7*, 665–669. [CrossRef]
90. Appiah, A.S.; Amoatey, H.M.; Klu, G.Y.P.; Afful, N.T.; Owusu, G.K. Spread of African cassava mosaic virus from cassava (*Manihot esculenta* Crantz) to physic nut (*Jatropha curcas* L.) in Ghana. *J. Phytol.* **2012**, *4*, 31–37.
91. Schmidt-Schultz, T.H.; Schultz, M. Bone protects proteins over thousands of years: Extraction, analysis, and interpretation of extracellular matrix proteins in archaeological skeletal remains. *Am. J. Phys. Anthropol.* **2004**, *128*, 30–39. [CrossRef] [PubMed]
92. Harper, E.; Kang, A.H. Studies on the specificity of bacterial collagenase. *Biochem. Bioph. Res. Co.* **1970**, *41*, 482–487. [CrossRef] [PubMed]
93. Dunn, K.A.; McLean, R.J.C.; Upchurch, G.R.; Folk, R.L. Enhancement of leaf fossilization potential by bacterial biofilms. *Geology* **1997**, *25*, 1119–1122. [CrossRef]
94. Child, A.M. Microbial taphonomy of archaeological bone. *Stud. Conserv.* **1995**, *40*, 19–30.
95. Retallack, G.J. Completeness of the rock and fossil record: Some estimates using fossil soils. *Paleobiology* **1984**, *10*, 59–78. [CrossRef]
96. Retallack, G.J. Dinosaurs and dirt. In *Dinofest International Proceedings*; Wolberg, D.L., Stump, E., Rosenberg, G.D., Eds.; Academy of Natural Sciences: Philadelphia, PA, USA, 1997; pp. 345–359.
97. Ullmann, P.V.; Shaw, A.; Nellermoe, R.; Lacovara, K.J. Taphonomy of the Standing Rock Hadrosaur Site, Corson County, South Dakota. *PALAIOS* **2017**, *32*, 779–796. [CrossRef]
98. Peterson, J.E.; Lenczewski, M.E.; Scherer, R.P. Influence of microbial biofilms on the preservation of primary soft tissue in fossil and extant archosaurs. *PLoS ONE* **2010**, *5*, e13334. [CrossRef]
99. Ullmann, P.V.; Macauley, K.; Ash, R.D.; Shoup, B.; Scannella, J.B. Taphonomic and diagenetic pathways to protein preservation, part I: The case of *Tyrannosaurus rex* specimen MOR 1125. *Biology* **2021**, *10*, 1193. [CrossRef]
100. Berner, R.A. Calcium carbonate concretions formed by the decomposition of organic matter. *Science* **1968**, *159*, 195–197. [CrossRef]
101. Allison, P.A. Konservat-Lagerstätten: Cause and classification. *Paleobiology* **1988**, *14*, 331–344. [CrossRef]
102. Briggs, D.E.G.; Kear, A.J. Fossilization of soft tissue in the laboratory. *Science* **1993**, *259*, 1439–1442. [CrossRef] [PubMed]
103. Sagemann, J.; Bale, S.J.; Briggs, D.E.G.; Parkes, R.J. Controls on the formation of authigenic minerals in association with decaying organic matter: An experimental approach. *Geochim. Cosmochim. Acta* **1999**, *63*, 1083–1095. [CrossRef]
104. Martin, D.; Briggs, D.E.G.; Parkes, R.J. Experimental attachment of sediment particles to invertebrate eggs and the preservation of soft-bodied fossils. *J. Geol. Soc.* **2004**, *161*, 735–738. [CrossRef]
105. Kral, A.G.; Ziegler, A.; Tütken, T.; Geisler, T. Experimental aqueous alteration of cortical bone microarchitecture analyzed by quantitative micro-computed tomography. *Front. Earth Sci.* **2021**, *9*, 609496. [CrossRef]
106. Kral, A.G.; Lagos, M.; Guagliardo, P.; Tütken, T.; Geisler, T. Rapid alteration of cortical bone in fresh- and seawater solutions visualized and quantified from the millimeter down to the atomic scale. *Chem. Geol.* **2022**, *609*, 121060. [CrossRef]
107. Trueman, C.N.; Martill, D.M. The long-term survival of bone: The role of bioerosion. *Archaeometry* **2002**, *44*, 371–382. [CrossRef]
108. Javan, G.T.; Finley, S.J.; Can, I.; Wilkinson, J.E.; Hanson, J.D.; Tarone, A.M. Human thanatomicrobiome succession and time since death. *Sci. Rep.* **2016**, *6*, 29598. [CrossRef]
109. Zhang, J.; Wang, M.; Qi, X.; Shi, L.; Zhang, J.; Zhang, X.; Yang, T.; Ren, J.; Liu, F.; Zhang, G.; et al. Predicting the postmortem interval of burial cadavers based on microbial community succession. *Forensic Sci. Int.-Gen.* **2021**, *52*, 102488. [CrossRef]
110. Delgado-Baquerizo, M.; Oliverio, A.M.; Brewer, T.E.; Benavent-González, A.; Eldridge, D.J.; Bardgett, R.D.; Maestre, F.T.; Singh, B.K.; Fierer, N. A global atlas of the dominant bacteria found in soil. *Science* **2018**, *359*, 320–325. [CrossRef]
111. Konhauser, K.O. Diversity of bacterial iron mineralization. *Earth-Sci. Rev.* **1998**, *43*, 91–121. [CrossRef]
112. Farmer, J. Taphonomic models in microbial fossilization. In *Size Limits of Very Small Organisms: Proceedings of a Workshop*; Farmer, J., Fogel, M.L., Lawrence, J., Lester, M.I., Olsen, G.J., Eds.; National Academy Press: Washington, DC, USA, 1999; pp. 94–102.
113. Liebig, K. Bacteria. In *Palaeobiology II*; Crowther, P.R., Ed.; Blackwell Publishing: Oxford, UK, 2001; pp. 253–256.
114. Hitchcock, A.P.; Dynes, J.J.; Lawrence, J.R.; Obst, M.; Swerhone, G.D.W.; Korber, D.R.; Leppard, G.G. Soft X-ray spectromicroscopy of nickel sorption in a natural river biofilm. *Geobiology* **2009**, *7*, 432–453. [CrossRef] [PubMed]
115. Elmore, K.L.; Hatfield, J.D.; Dunn, R.L.; Jones, A.D. Dissociation of phosphoric acid solution at 25°. *J. Phys. Chem.* **1965**, *69*, 3520–3525. [CrossRef]
116. Toporski, J.K.W.; Steele, A.; Westall, F.; Avci, R.; Martill, D.M.; McKay, D.S. Morphological and spectral investigation of exceptionally well-preserved bacterial biofilms from the Oligocene Enspel Formation, Germany. *Geochim. Cosmochim. Acta* **2002**, *66*, 1773–1791. [CrossRef]
117. Atkins, P.; Jones, L. *Chemical Principles*, 5th ed.; W.H. Freeman and Company: New York, NY, USA, 2009; pp. 1–1024.
118. Schweitzer, M.H.; Schroeter, E.R.; Cleland, T.P.; Zheng, W. Paleoproteomics of Mesozoic dinosaurs and other Mesozoic fossils. *Proteomics* **2019**, *19*, 1800251. [CrossRef]

119. Fernández-Jalvo, Y.; Andrews, P.; Pesquero, D.; Smith, C.; Marín-Monfort, D.; Sánchez, B.; Geigl, E.-M.; Alonso, A. Early bone diagenesis in temperate environments Part I: Surface features and histology. *Palaeogeogr. Palaeocl.* **2010**, *288*, 62–81. [CrossRef]
120. Trueman, C.N.G.; Behrensmeyer, A.K.; Tuross, N.; Weiner, S. Mineralogical and compositional changes in bones exposed on soil surfaces in Amboseli National Park, Kenyz: Diagenetic mechanisms and the role of sediment pore fluids. *J. Archaeol. Sci.* **2004**, *31*, 721–739. [CrossRef]